NUMERICAL CALCULATION OF ROUGH TURBULENT BOUNDARY LAYER FOR INCOMPRESSIBLE FLUIDS

A THESIS SUBMITTED TO
THE GRADUATE SCHOOL OF APPLIED AND NATURAL SCIENCES
OF
MIDDLE EAST TECHNICAL UNIVERSITY

BY

GÖRKEM ATAY

IN PARTIAL FULFILLMENT OF THE REQUIREMENTS
FOR
THE DEGREE OF MASTER OF SCIENCE
IN
MECHANICAL ENGINEERING

SEPTEMBER 2018

Approval of the thesis:

NUMERICAL CALCULATION OF ROUGH TURBULENT BOUNDARY LAYER FOR INCOMPRESSIBLE FLUIDS

submitted by **GÖRKEM ATAY** in partial fulfillment of the requirements for the degree of **Master of Science in Mechanical Engineering Department, Middle East Technical University** by,

Prof. Dr. Halil Kalıpçılar
Dean, Graduate School of **Natural and Applied Sciences** _____

Prof. Dr. M. A. Sahir Arıkan
Head of Department, **Mechanical Engineering** _____

Asst. Prof. Dr. Özgür Bayer
Supervisor, **Mechanical Engineering Dept., METU** _____

Prof. Dr. Cahit Çıray
Co-supervisor, **Aerospace Engineering Dept., METU** _____

Examining Committee Members:

Assoc. Prof. Dr. Cüneyt Sert
Mechanical Eng. Dept., METU _____

Asst. Prof. Dr. Özgür Bayer
Mechanical Eng. Dept., METU _____

Prof. Dr. Cahit Çıray
Aerospace Eng. Dept., METU _____

Asst. Prof. Dr. Özgür Uğraş Baran
Mechanical Eng. Dept., METU _____

Asst. Prof. Dr. Rahim Jafari
Automotive Eng. Dept., AU _____

Date: 03.09.2018

I hereby declare that all information in this document has been obtained and presented in accordance with academic rules and ethical conduct. I also declare that, as required by these rules and conduct, I have fully cited and referenced all material and results that are not original to this work.

Name, Last Name: GÖRKEM ATAY

Signature:

ABSTRACT

NUMERICAL CALCULATION OF ROUGH TURBULENT BOUNDARY LAYER FOR INCOMPRESSIBLE FLUIDS

Atay, Görkem
M.S., Department of Mechanical Engineering
Supervisor: Asst. Prof. Dr. Özgür Bayer
Co-supervisor: Prof. Dr. Cahit Çıray

September 2018, 81 pages

In this thesis, a numerical code for calculating turbulent boundary layer parameters is developed. Two-dimensional turbulent flow over a rough flat plate with zero pressure gradient is numerically solved by using the integral method. Fluid mechanics formulations, such as momentum integral equation are coupled with the results of Nikuradse's experiment. Throughout the calculation, turbulent boundary layer parameters, such as boundary layer thickness, displacement thickness, momentum thickness, local skin-friction coefficient etc. are obtained.

Development of turbulent boundary layer (TBL) is taken into consideration in the present study. This notion is quite important in terms of accuracy of the calculation of TBL parameters. Because, flow conditions may change from fully-rough flow to hydraulically smooth flow, and this may reduce the drag force severely. For a precise TBL solution, the calculation method considers the relative size of the TBL sublayers thicknesses and the surface roughness height with respect to each other at every

computation step along the developing TBL. Furthermore, one of the parameters of TBL is the wake parameter and has a vital importance in the calculations. It is at the same time a function of TBL thickness, local skin-friction coefficient and surface roughness. By using a method developed during this study, wake parameter is computed and embedded into the relevant equations at every solution-point on the calculation domain.

The developed code is tested against experimental data, a numerical study in the literature and Schlichting skin-friction formula. Generally, the full flow conditions are not detailed in the experimental cases found in the literature. Hence, the comparisons are reliable much more on the cases for which full details were available. The developed code shows very good agreement within its range. For the fully-rough flow regime, the present study's relative mean discretization error in C_f is 0.6% whereas it is 2.1% for the numerical study in the literature. For the transition flow regime, the relative mean discretization error in C_f is found to be 1.9% in the present work and it is 8.0% for the numerical study in the literature.

Keywords: Turbulent Boundary Layer, Surface Roughness, Numerical, Skin-Friction Coefficient.

ÖZ

TÜRBÜLANSLI SINIR TABAKANIN SIKIŞTIRILAMAZ AKIŞKANLAR İÇİN SAYISAL OLARAK HESAPLANMASI

Atay, Görkem
Yüksek Lisans, Makina Mühendisliği Bölümü
Tez Danışmanı: Dr. Öğ. Üy. Özgür Bayer
Ortak Tez Danışmanı: Prof. Dr. Cahit Çıray

Eylül 2018, 81 sayfa

Bu tezde, türbülanslı sınır tabakaya ait çoklukları hesaplayan sayısal bir kod geliştirilmiştir. İki boyutlu türbülanslı akım, üzerinde basınç değişimi olmayan pürüzlü düz plakalar için, integral metotu kullanılarak çözülmüştür. Momentum integral denklemi gibi akışkanlar mekaniği formülleri, Nikuradse'nin deneysel sonuçları ile birleştirilmiştir. Hesaplama boyunca, türbülanslı sınır tabakaya ait; sınır tabaka kalınlığı, yer değiştirme kalınlığı, momentum kalınlığı, yerel yüzey-sürtünme katsayısı ve benzeri çokluklar elde edilmiştir.

Türbülanslı sınır tabakasının (TST) gelişimi gerçekleştirilen çalışmada dikkate alınmıştır. TST çokluklarının doğrulukla hesaplanması açısından bu değerlendirme yaklaşımı oldukça önemlidir. Çünkü, akım koşulları tam pürüzlü akımdan hidrolikli pürüzsüz akıma değişebilir, ve bu durum sürükleme kuvvetinin oldukça azalmasına neden olabilir. Hassas bir TST çözümü için, hesaplama yöntemi TST'ye ait alt sınır tabaka kalınlıklarının ve yüzey pürüzlülüğü yüksekliğinin birbirlerine göre olan göreceli büyüklüklerini her hesaplama adımında göz önünde bulundurmaktadır. Buna

ilaveten, TST çokluklarından bir tanesi olan profil parametresi, TST'ye ait parametrelerin hesaplanmasında oldukça önem taşımaktadır. Profil parametresi aynı zamanda TST kalınlığının, yüzey-sürtünme katsayısının ve yüzey pürüzlülüğünün bir fonksiyonudur. Profil parametresi, çalışma süresince geliştirilen bir yöntem ile hesaplama ağının her çözüm noktasında elde edilmiş ve ilgili denklemlerin içerisine yerleştirilmiştir.

Geliştirilen kod; deneysel veriler, literatürdeki sayısal bir çalışma ve Schlichting'in yüzey-sürtünmesi formülasyonu ile test edilmiştir. Literatürden elde edilmiş deneysel çalışmalarda, akım koşulları genelde detaylı olarak verilmemiştir. Bundan dolayı, akım koşullarının detaylı olarak sunulduğu deneysel çalışmalar ile gerçekleştirilen karşılaştırmalar daha güvenilirdir. Geliştirilen kod, çalışma limitleri içerisinde oldukça tatmin edici sonuçlar vermiştir. Tam-pürüzlü akım bölgesinde yüzey pürüzlülük katsayısındaki ortalama bağıl hata gerçekleştirilen çalışma için %0.6 iken, bu değer literatürdeki sayısal çalışma için %2.1'dir. Geçiş akım bölgesi için ise, yüzey pürüzlülük katsayısındaki ortalama bağıl hata gerçekleştirilen çalışma için %1.9 olarak hesaplanırken, literatürdeki sayısal çalışma için %8.0 olarak bulunmuştur.

Anahtar Kelimeler: Türbülanslı Sınır Tabaka, Yüzey Pürüzlülüğü, Sayısal, Yüzey-Sürtünme Katsayısı.

This study is dedicated to future researchers and to people who make the world worth living…

ACKNOWLEDGEMENTS

I would like to thank my supervisor Asst. Prof. Dr. Özgür BAYER for his, guidance, patience and contribution during this study. He always keeps me going further and further with his inexhaustible support.

I also would like to deeply express my endless thankfulness to my co-supervisor Dear Prof. Dr. Cahit ÇIRAY for his continuous support of my MS-study with his immense knowledge, experience, perfect guidance, and encouragement. I feel myself fortunate to get chance to meet with him. He always kept my motivation as possible as high, and his door was always open to me whenever I got issue stacked in my mind. Working with him was honorary for me…

Finally, I convey my sincere thanks to my colleagues Aykut Barış İNCİ and Tuğcan SELİMHOCAOĞLU who encourage me a lot and share their unfailing experience during my thesis period.

TABLE OF CONTENTS

LIST OF TABLES

TABLES

LIST OF FIGURES

FIGURES

LIST OF SYMBOLS

Roman Symbols

A, B	Smooth wall intercept constant [/]
A'	Rough wall intercept constant [/]
b	$(1 + \epsilon_m^+)$ [/]
C_1	$\int_0^1 f(\eta) d\eta$ [/]
C_2	$\int_0^1 f^2(\eta) d\eta$ [/]
C_f	Skin-friction coefficient [/]
C_{f_comp}	C_f values that are compared with the experiment results [/]
C_{f_ctrl}	C_f value to check the calculated C_f value whether it is true or not [/]
C_{f_exp}	C_f values obtained from the experimental results [/]
C_D	Drag coefficient [/]
Δx	Grid length [m]
F_1	Roughness factor [/]
F_2	Pressure gradient factor [/]
f	Velocity-defect law [/]
fr	Frequency [Hz]
fr_D	Frequency of minimum energy in energy spectrum [Hz]
fr_E	Frequency of maximum energy in energy spectrum [Hz]
g	Functional dependence [/]
H	Shape parameter [/]
H_1	Shape factor [/]
k_s	Equivalent sand roughness [m]
L	Length of the plate's portion interested in fully-turbulent flow [m]
l_m	Mixing length [m]
M	Momentum [kg m/s]

m	Pressure gradient parameter [/]
$\dot{m}$	Mass flow [kg/s]
n	Semiempirical constant depending on Re [/]
Re	Reynolds number [/]
Re_{δ_1}	Displacement thickness Reynolds number [/]
Re_{δ_2}	Momentum thickness Reynolds number [/]
S_1	Semiempirical constant depending on Re [/]
U	Velocity component in x-direction (Streamwise direction) [m/s]
U_τ	Friction velocity [m/s]
$-\overline{uv}$	Turbulent (or Reynolds) shear stress [m^2/s^2]
V	Velocity component in y-direction (wall normal direction) [m/s]
W	Wake function [/]
x	Cartesian, spatial coordinate for streamwise direction [m]
y	Cartesian, spatial coordinate for wall normal direction [m]

Greek Symbols

γ, Ψ	Similarity parameters [/]
ΔU_1	Roughness contribution to logarithmic-law, empirical [m/s]
ΔU_2	Pressure gradient contribution to velocity-defect law, empirical [m/s]
ΔU^+	Roughness function [/]
δ	Boundary layer thickness [m]
δ_1	Displacement thickness [m]
δ_2	Momentum thickness [m]
ϵ_m	Eddy viscosity [m^2/s]
η	y/δ [/]
κ	von Kármán constant [/]
λ	Skin-friction factor [/]
ν	Kinematic viscosity [m^2/s]
Π	Pressure term divided by density [J/kg]
ρ	Density [kg/m^3]
τ	Shear stress [kg m^2/s^2]

ϖ	Wake parameter [/]

Mathematical Operators

d	Ordinary derivative operator
∂	Partial derivative operator

Subscripts

E	Edge conditions at a specific x location in the boundary layer
T	Representing the turbulent quantities
tot	Total
v	Representing the viscous quantities
w	Wall conditions at a specific x location in the boundary layer
SP	Solution-points
OP	Output-points

Superscript

+	Nondimensionalization with $U_\tau, U_\tau/\nu$ or ν

Special Symbol

$\bar{A}$	Reynolds averaging of a quantity (A)

LIST OF ABBREVIATIONS

2D	Two-dimensional
3D	Three-dimensional
BL	Boundary Layer
CFD	Computational Fluid Dynamics
ENC	Electronic Numerical Calculator
GIS	Grid Independence Study
LF	Laminar Flow
OP	Output-Point
PDE	Partial Differential Equation
RAM	Random Access Memory
RANS	Reynolds Averaged Navier Stokes
Re	Reynolds Number
RMDE	Relative Mean Discretization Error
SP	Solution-Point
TBL	Turbulent Boundary Layer
TEE	Turbulent Energy Equation
TF	Turbulent Flow
TKE	Turbulent Kinetic Energy
TML	Turbulent Mixing Length
UER	Universal Equilibrium Range
wrt	With Respect To

CHAPTER 1

INTRODUCTION

1.1 Highlights of Drag Force and Boundary Layer Theory

All kind of fluid flows over solid bodies, such as air flows around automobiles, motorcycles, airplanes, zeppelins, missiles, submarines, are designed to produce minimum drag force. This is one of the most important problems of a modern design process. Producing solutions to such problems result in industrial gains. Obtaining high velocities, reduction in fuel consumption, aircraft with stealthy characteristics can be given as examples [1]. Figuring out the physical phenomenon behind external flows improves the design capability. Thus, it is possible to design any geometry, which is exposed to flow more efficiently in terms of both aerodynamics and cost.

It is well known that any object moving in a fluid encounters a resistance. This resistance results in drag force which is composed of pressure and frictional components on a solid body. A part of the drag force of a body due to frictional stresses is referred to skin-friction drag [2]. The drag is not a desired effect and it should be maintained at a minimum level. Nevertheless, in some cases, drag is helpful like in the case of parachute effect.

Hence, understanding the drag phenomenon before improving the aerodynamic design of an object is essential and it can be achieved by conceiving the boundary layer (BL) theory.

To solve BL and obtain the interested values belong it, Navier-Stokes equations (conservation of linear momentum equations) took place in the scientific world both theoretically and experimentally through the end of the nineteenth century. For some flows, these equations can be solved and their validation with experiments was done. But, velocities at the solid boundary is a controversial topic. For low-speed flows, the velocities at the solid boundary are accepted to be zero, but for high-speed flows, there are some who claim that velocity at the solid boundary has a finite value [3]. L. Prandtl is the first academician who enlightened the physical background of a flow in the vicinity of the solid surface. According to the Prandtl's study; there is a layer that is thin and close to the solid boundary in which the viscosity is dominant and the flow out of this layer can be considered as irrotational [3]. In the outer layer, there exist no large velocity gradients and the effectiveness of viscosity is insignificant [4].

The exact solution of L.Prandtl equations for a laminar boundary layer approach was first done by his student, H. Blasius in 1908. Because the solution is not handy to use, Prandtl boundary layer theory was drawn attention by neither mathematicians nor engineers. In 1921, Theodore von Kármán introduced the momentum integral equation. In the same year, K. Pohlhausen gave a practical way to solve this equation and finally, the boundary layer and its theory attracted the expected interest [3].

It is known that the BL theory can be applied not only to laminar flows (LF) but also to turbulent flows (TF) [3].

There are significant distinctions between the characteristics of laminar and turbulent boundary layers (TBL). One of the differences between them is; an ordinary TBL velocity profile on a flat plate at zero pressure gradient is more uniform throughout its thickness except for adjacent to the solid boundary. Hence, the velocity gradient at the solid surface is much higher in the TF than in the LF. Since the frictional stress (or shear stress) at the wall is proportional to this velocity gradient, frictional stress or drag is generally much higher in TF than that of laminar one [2].

The drag force is affected by the surface condition as well, which can be smooth or rough. A smooth surface in contact with the fluid is generally considered as the surface of glass or polished timber material. In reality, even these surfaces have very small protrusions.

For the rough surface, the frictional drag force is larger compared to that of the smooth one. This is because small roughness elements behave like bluff bodies and eddies are pushed out which disrupt the laminar boundary layer and provoke transition to TF resulting in a boost in drag force. If the roughness elements are larger, its effect on drag force is higher as shown in Figure 1.1 [2].

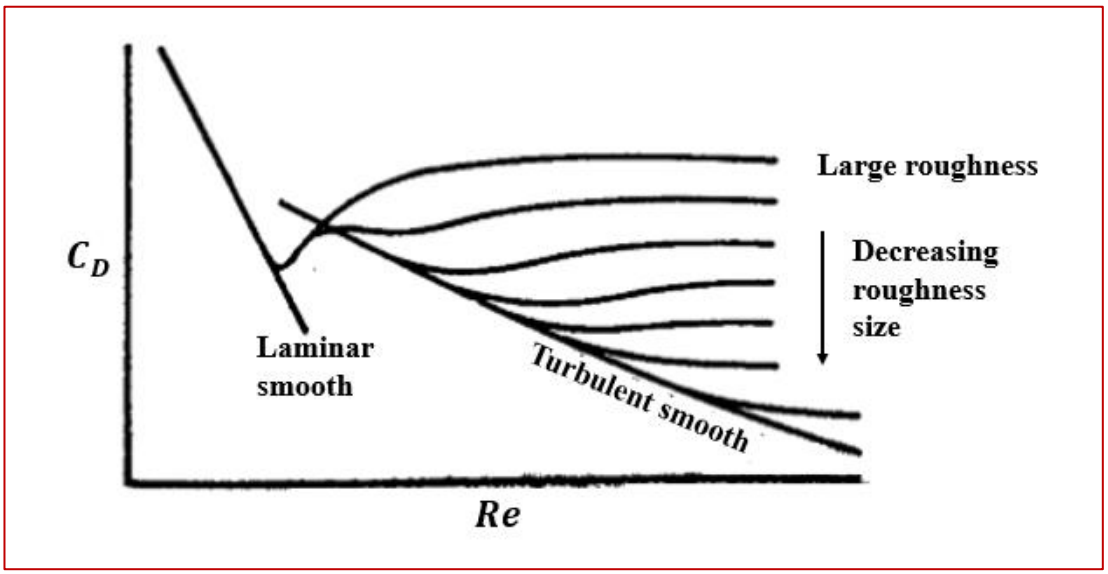

Figure 1.1 Variation of drag coefficient with respect to Reynolds number for different roughness height on a flat plate at zero incidence [2]

1.2 Highlights of the Methods to Solve Boundary Layer Equations

Even a slight decrease in the drag-count is a desired objective in the fluid mechanics field and industry. One way to accomplish this is to reduce the skin-friction drag on the objects (such as aircraft, automobiles etc.). There are a number of methods which

decrease the skin-friction drag, such as extension of LF, relaminarization of TF, modification to the turbulence characteristics of the flow adjacent to the wall [5].

During a numerical solution, the skin-friction drag can be obtained by means of a more precise BL calculation. Hence, it is important to perform an as much as possible correct BL computation at a design phase. Today there are mainly two types of methods which help to calculate the BL numerically.

Since the capability of the computers in solving a complex system of partial differential equations (PDEs) raised in the 1960s, the attention in the solution of TBL equations in their partial differential form has increased. Consequently, differential methods have been developed and used since that time [6].

The differential method is composed of two different approaches. One of them is the mean-flow approach and the other one is the transport-equation approach [6]. For the transport-equation treatment; mean continuity equation, mean momentum and the converted form of turbulent kinetic energy (TKE) equations create a hyperbolic system together, and by solving this system of equations, TBL parameters can be obtained. In the mean-flow approach of the differential method, parameters of TBL can be acquired by using only mean continuity and mean momentum equations. For the solution procedure, in general, the pressure change in the flow direction should be known and an appropriate turbulence model should be used for the turbulence stress term in the TBL equations. Both solution technics has superiority with respect to each other.

On the other hand, before the high-speed computers became prevalent, the integral methods were used for the BL calculation. Therefore, mathematical difficulties to solve the nonlinear BL equations in their partial differential form were avoided [6]. According to Schlichting [4], a full calculation of a BL for a given object with the aid of differential equations is so complex and time-consuming that it is not logical to carry out in practical life. Hence, it is desired to find an approximate method for the solution of BL. Such methods can be taken into consideration if one does not try to provide differential equations for every fluid particle and deals only with the mean

values of a BL parameters. This kind of mean value can be acquired from the momentum integral equation that is obtained from the equation of motion by integrating throughout the boundary layer thickness. The momentum integral approach is one of the approximate methods to predict the boundary layer's parameters which are interested in engineering purposes.

Some studies related to the calculation of TBL or merely the skin-friction coefficient, C_f, are presented in Section 1.4.

1.3 Motivation of the Present Study

In the present study, it is focused to obtain a numerical code which calculates the TBL parameters as accurate as possible for incompressible, two-dimensional, steady-state turbulent flow over a rough surface with zero pressure gradient. Throughout the numerical calculation, integral method is used.

One of the most important characteristics of the present study is that the solution technique considers the TBL developing. According to such consideration, the relative size of sublayers thicknesses in a TBL and surface roughness height with respect to each other is a crucial matter to obtain the correct values of TBL parameters. As a result of this notion, TBL parameters can be obtained more precisely.

Another important characteristic of the present work is that the fluid mechanics formulations, such as momentum integral equation, is coupled with the results of Nikuradse's experiment. These formulations form a different system of equations compared to the studies in the literature for the solution of TBL parameters.

In the literature review of TBL calculation studies where the integral method is used, most of the time momentum integral formulation forms a closed system of equations with the additional relations to equalize the number of unknowns and equations to obtain the TBL parameters. According to Cebeci [6], there is not universal relationship between them, and hence assumptions should be made. As a result, the accuracy of the

calculation of TBL parameters highly relies on the assumptions. Examples from the literature which are about the numerical calculation of TBL by using the integral method is presented in Section 1.4.

The detailed explanation related to the consideration which takes into account the TBL developing are given in the following paragraphs.

In a TBL there are three sublayers named; viscous sublayer, buffer layer and fully turbulent layer as shown in Figure 1.2. In a viscous sublayer, the viscosity is dominant, and the effect of the turbulence can be neglected compared to that of viscous effects. In a buffer layer; whereas viscous effects are dominant at the lower limit of this layer, at the upper limit of it, turbulence effects are prevailing. In a fully turbulent layer, almost only the turbulence effects are determinant on the flow character.

There are principally three types of flow regime on a rough solid surface. These are; hydraulically smooth, transition and fully-rough flow regimes.

The flow type is determined with respect to the region where the roughness elements are confined in the TBL sublayers as shown in Figure 1.2. In the hydraulically smooth flow, the viscous sublayer is assumed to be thick enough such that roughness remains in this layer. Hence the fluid particles move through the rough elements smoothly and the flow is not affected by roughness like domain-3 in Figure 1.2. Thus, in the viscous sublayer, flow parameters are the only a function of Reynolds number (Re). In the transition regime, the roughness remains in the buffer layer and affects the flow like domain-2 in Figure 1.2. Thus, the flow parameters are a function of both the Re and the roughness. Finally, if the roughness remains in the fully turbulent layer, the flow parameters are the only a function of roughness and not Re like domain-1 in Figure 1.2. This regime is called “hydraulically rough flow” [7].

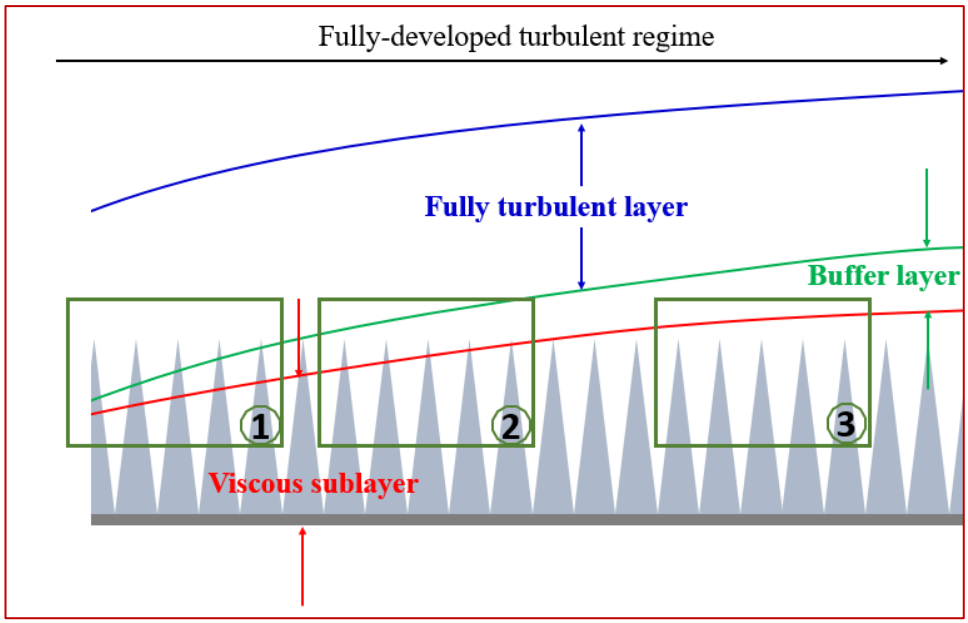

Figure 1.2 Variation of relative thicknesses of TBL sublayers and the roughness height (schematic)

According to the explanations above, drag may be affected by the surface roughness and the more realistic drag force on a solid body in a fluid flow can be obtained when the more precise skin-friction coefficient is used in both analytical or numerical calculations.

The mathematical model used in the present study to calculate TBL parameters, which is explained detailed in CHAPTER 2, considers relative size of sublayers thicknesses in a TBL and surface roughness height with respect to each other at every calculation step. This is because thicknesses of TBL sublayers are increasing in flow direction. As a result, roughness elements which are in fully turbulent layer at the beginning of a flat plate may lie within viscous sublayer after some distance away. Such a situation causes a dramatic decrease in C_f value. Hence, a control mechanism that checks where roughness elements are in TBL is used for every solution-point in the present study.

In the computational domain, any points in fully-developed turbulent regime of flow can be selected as a starting point for the TBL calculation.

1.4 Literature Review

Former TBL calculation over rough flat plates started with analytical and experimental studies.

In 1911, Blasius made a very significant study on pipe flow [4]. He obtained an empirical skin-friction factor named "Blasius formula", Eqn. (1.1), for the pipe flow by using numerous experimental results and arranging them in the dimensionless form resembling Reynolds' similarity law.

$$\lambda = \frac{0.3164}{\mathrm{Re}^{0.25}} \tag{1.1}$$

where;

λ : skin-friction factor.

On the other hand, Nikuradse conducted an experimental investigation into the law of friction and velocity distribution in smooth pipes [4]. As a result, he introduced an empirical velocity distribution equation named power-law:

$$\frac{\overline{U}(y)}{U_\tau} = S_1\left(\frac{yU_\tau}{\nu}\right)^{1/r} \tag{1.2}$$

where;

U : velocity distribution in streamwise direction,

U_τ : friction velocity, which is used in nondimensionalization operation,

y : cartesian, spatial coordinate for wall normal direction,

ν : fluid kinematic viscosity,

S_1 : semiempirical constant depending on Re,

r : semiempirical constant depending on Re.

The power-law equation and the Blasius formula are related to each other. Such a relationship is first discovered by Prandtl and allowed him to draw a conclusion from pipe experiments which are valid for the flat plate [8].

The relationship between pipe flows and boundary layer flows is necessary. Because in many cases, such as flow over aircraft or ships, the Re is so high that it cannot be measured in a laboratory. Furthermore, even at moderate Re number, it is still hard to measure boundary layer characteristics on a flat plate compared to measuring boundary layer characteristics inside a pipe. Hence, by means of pipe experiments results, skin-friction coefficient on a flat plate can be obtained for high Re by using the method of Prandtl. The calculation is available for both smooth and rough surfaces [4].

In the light of the information, Prandtl and Schlichting performed the earliest calculation of two-dimensional TBL on a smooth surface for moderate Re. The calculation procedure depends on the analogy between the pipe flow and the boundary layer flow by assuming the velocity profile on a flat plate is identical with that of the inside of a circular pipe. The assumption well meets with the experimental studies conducted by Burgers and Hansen [9] at least for moderate Re.

Prandtl's and Schlichting's work distinguished by the result that the velocity profile in a pipe flow can be used for the flat plate by applying a power formula, Eqn. (1.2) [4]. After having obtained the integral parameters belong to TBL by means of Eqn. (1.2) and the formulation of momentum thickness and displacement thickness, the skin-friction coefficient is derived by using momentum integral equation. Eventually, substituting the proper values of C_1 and n; the local C_f formulation turns out to be:

$$C_f = 0.0576\mathrm{Re}^{\frac{-1}{5}} \qquad 5\times10^5 < \mathrm{Re} < 10^7 \tag{1.3}$$

For the high Re fluid flow, Prandtl used power-law velocity distribution instead of using logarithmic-law. This is because logarithmic-law can be considered as an asymptotic law which is applicable to very large Re by means of extrapolation. Hence performing experiments for high Re is not required, in contrast with power-law. As mentioned, the calculation of skin-friction for high Re flow depends on pipe experiments results. With the help of a mathematical method of Prandtl, skin-friction

coefficient on a flat plate was achieved as a function of Re and presented in a table [10].

The results were evaluated as exceedingly inconvenient. Hence, Schlichting put the Prandtl's relation between C_f and Re into an empirical equation for smooth surfaces and named it "Prandtl-Schlichting skin-friction formula for a smooth flat plate at zero incidences" [10].

$$C_f = 0.455(\log \mathrm{Re})^{-2.58} \qquad 5\times10^5 < \mathrm{Re} < 10^9 \tag{1.4}$$

Its version for a rough surface is:

$$C_f = \left(2.87 + 1.58 \log \frac{x}{k_s} \right)^{-2.5} \qquad k_s^+ > 70 \ \text{ and } \ 10^2 < \left(x / k_s \right) < 10^6 \tag{1.5}$$

where;

x : cartesian, spatial coordinate for streamwise direction,

k_s : equivalent sand roughness, defined as defined as diameter of sand grains which create same drag effect with surface roughness interested.

Although logarithmic-law based C_f formulations, Eqn. (1.4) and Eqn. (1.5), are widely used, they are still overestimating the C_f value compared to experimental results.

According to the measurement of the boundary layer on a plate, as shown in Figure 1.3, Schultz-Grunow states that the velocity profile in the outer portion (shown as outer layer in Figure 1.4) of the boundary layer of a plate deviates from the logarithmic velocity distribution inside a circular pipe.

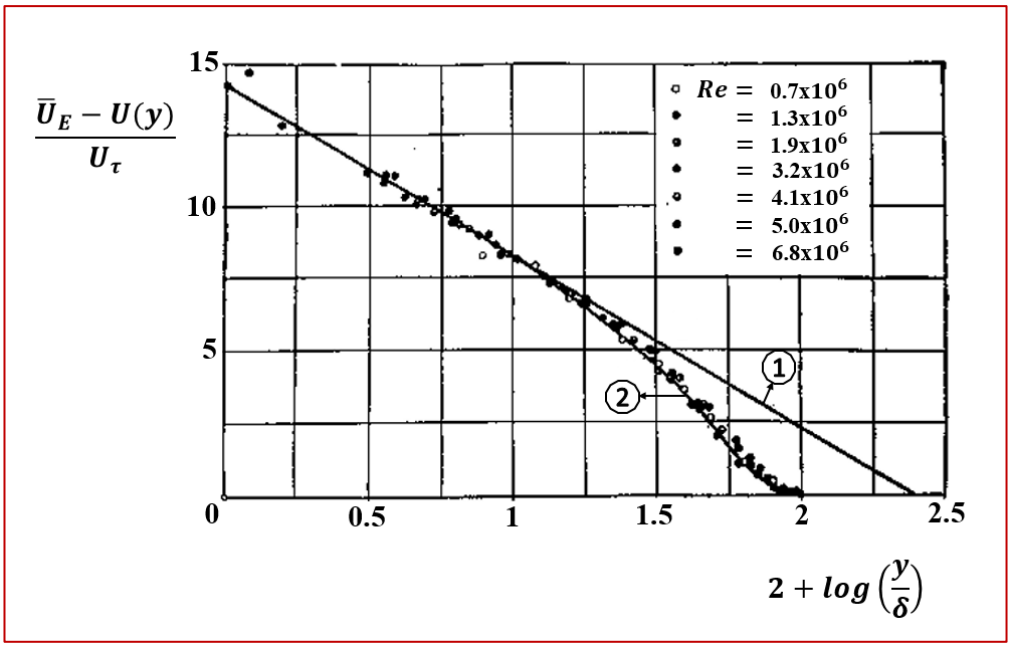

Figure 1.3 Velocity distribution in the boundary layer on a flat plate at zero incidence after Schultz-Grunow [4]; curve (1) and (2) stands for the circular pipe and plate respectively

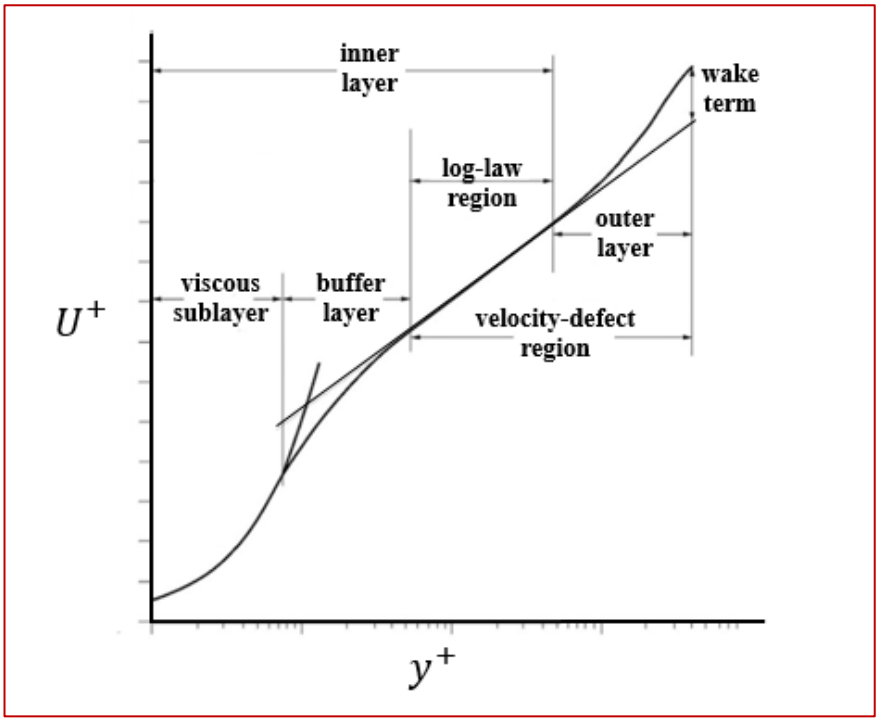

Figure 1.4 Velocity distribution in TBL for a flat plate

Therefore, F. Schultz-Grunow suggested new formulations for the mean and the local skin-friction coefficients by using the same system of equation that Schlichting used. However, F. Schultz-Grunow took also velocity measurement results in the boundary layer on a flat plate at zero incidence into consideration, as shown in Figure 1.3. The suggested local skin-friction coefficient for smooth surfaces is presented in the Eqn. (1.6).

$$C_f = 0.370\left(\log \mathrm{Re}\right)^{-2.584} \tag{1.6}$$

Another important subject concerning the physical problem in the literature is the numerical calculation of TBL in which either integral or differential method is used. Such studies are conducted for the flow over a smooth and rough surface with and without a pressure gradient. Furthermore, whereas some of them consider the main three regimes (named hydraulically smooth, transition and fully-rough flow), others take into account only the fully-rough flow regime.

In the Bettermann's study [11], he used the integral method to calculate the skin-friction coefficient of turbulent flow over a rough and smooth surface with zero pressure gradient. Furthermore, he performed his work for the fully-rough flow regime.

For the smooth surface, he used the formulation:

$$\frac{U}{\overline{U}_E} = 5.6\sqrt{\frac{C_f}{2}}\log\frac{y\overline{U}_E}{\nu} + 5.6\sqrt{\frac{C_f}{2}}\left(\log\sqrt{\frac{C_f}{2}} + 0.928\right) \tag{1.7}$$

where;

x : cartesian, spatial coordinate for streamwise direction,

$\overline{U}_E$: free-stream velocity.

If the values of $U/\bar{U}_E$ is drawn as a function of $y\bar{U}_E/\nu$, Eqn. (1.7) can be represented by a family of lines. Then, the local skin-friction coefficient is calculated from the slope of the lines.

And for the rough surface, he used the equation:

$$\frac{U}{\overline{U}_E} = 5.6\sqrt{\frac{C_f}{2}}\log\frac{y\bar{U}_E}{\nu} + \sqrt{\frac{C_f}{2}}\left(5.6\log\sqrt{\frac{C_f}{2}} + 5.2 - \frac{\Delta U_1}{U_\tau}\right) \tag{1.8}$$

where;

ΔU_1 : roughness contribution to logarithmic-law, empirical.

After having determined the values of $\Delta U_1/U_\tau$ experimentally, the same procedure used in the case of the smooth surface can be applied for the Eqn. (1.8). To check the value of the obtained skin-friction coefficient Eqn. (1.9) is used.

$$\frac{d\delta_2}{dx} = \frac{C_f}{2} \tag{1.9}$$

where;

δ_2 : momentum thickness.

Another study for the calculation of TBL parameters over a smooth surface with a pressure gradient depends on Head's technique which presents the integral method.

$$\frac{d\delta_2}{dx} + \frac{\delta_2}{\overline{U}_E}\frac{d\bar{U}_E}{dx}(H+2) = \frac{C_f}{2} \tag{1.10}$$

where;

H : shape parameter, δ_1/δ_2.

In the Eqn. (1.10), there are three unknowns; δ_2, H and C_f for a given velocity distribution. To solve the Eqn. (1.10), two more relations are necessary. Since there is

not a universal relationship among them, assumptions should be made. As a result, the precision of the solution of Eqn. (1.10) highly depends on the assumptions [6].

According to Head's method, the first relationship is:

$$\frac{d}{dx}\left(\overline{U}_E\,\delta_2\,H_1\right)=\overline{U}_E\,F \tag{1.11}$$

where;

$$H_1=G\left(H\right) \tag{1.12}$$

$$F=0.0306\left(H_1-3.0\right)^{-0.6169} \tag{1.13}$$

$$G=\begin{cases}0.8234\left(H-1.1\right)^{-1.287}+3.3 & H\le 1.6\\ 1.5501\left(H-0.6778\right)^{-3.064}+3.3 & H\ge 1.6\end{cases} \tag{1.14}$$

and the last relationship is:

$$C_f=0.246\times 10^{0.678H}\,\mathrm{Re}_{\delta_2}{}^{-0.268} \tag{1.15}$$

For a given free-stream velocity ($\overline{U}_E$) and the values of δ_2, H, C_f, TBL parameters can be calculated numerically by using the three main equations, Eqn (1.10), Eqn (1.11), Eqn. (1.15) [6].

Dvorak [12] performed the calculation of TBL on a rough surface in the pressure gradient. In the calculation procedure, momentum integral method was used and attempted to extend the applicability of Bettermann's [13] skin-friction law to a wider range of roughness shapes, to nonzero pressure gradient and to the transition regime.

In the calculation procedure, Eqn. (1.10), Eqn. (1.11) and Eqn. (1.16) are integrated simultaneously. For the values of $F, G, \Delta U_1$ and ΔU_2, the original paper should be referred.

$$\sqrt{\frac{2}{C_f}} = 5.6 \log \frac{\overline{U}\delta_1}{\nu} + 4.8 - \frac{\Delta U_1}{U_\tau} + \frac{\Delta U_2}{U_\tau} \tag{1.16}$$

where;

ΔU_2 : pressure gradient contribution to velocity-defect law, empirical.

The comparison with experiments is good in general. However, roughness shapes are limited to two-dimensional types of roughness and distributed sand.

Arndt and Ippen [14] also considered turbulent flow over a rough flat plate with a pressure gradient in which the momentum integral method is used. In their study, the pressure gradient term took part in their skin-friction law which is presented as:

$$\sqrt{\frac{2}{C_f}} = 5.6 \log \left(\frac{F_2}{F_1} \right) \frac{\overline{U}_E \, \delta_1}{\nu} + 4.5 \tag{1.17}$$

where;

F_1 : roughness factor,

F_2 : pressure gradient factor.

The skin-friction coefficients which are obtained by using this technique are compared with the ones which are achieved by the standard von Kármán momentum integral technique. The agreement is good. Unfortunately, the functions F_1 and F_2 must be experimentally determined in addition to displacement thickness Re (Re_{δ_1}), that is $\overline{U}_E \delta_1 / \nu$.

In the Cebeci and Keller's study [15], they used the differential method to solve the TBL and their method is used for several boundary layer applications. In the solution procedure, Falkner-Stan transformation was applied to the TBL equations to provide

a mathematical suitableness for the calculation technic. By means of a similarity parameter, Eqn. (1.18) and a dimensionless stream function, Eqn. (1.19), and with the definition of the eddy viscosity,

$$\gamma = y\sqrt{\frac{\overline{U}_E}{\nu x}} \tag{1.18}$$

$$\psi = \sqrt{\frac{\overline{U}_E}{\nu x}}\, g(x,\gamma) \tag{1.19}$$

Prandtl's BL equations for TF can be written in the form:

$$\left(bg^{"}\right)^{'} + \frac{m+1}{2} g g^{"} + m[1-(g^{'})^2] = x\left(g^{'}\frac{\partial g^{'}}{\partial x} - g^{"}\frac{\partial g}{\partial x}\right) \tag{1.20}$$

where;

b : $(1+\epsilon_m^+)$,

g : functional dependence,

ϵ_m : eddy-viscosity,

ϵ_m^+ : ϵ_m/ν,

m : pressure gradient parameter.

The solution of Eqn. (1.20) can be achieved by subjecting it the proper boundary conditions.

In their study, a modified version of the Coles' velocity profile was used and for a given skin-friction coefficient (C_f) and momentum thickness Re (Re_{δ_2}), boundary layer thickness (δ) and the wake parameter (ϖ) are obtained.

Cebeci and Chang also performed numerical work [16]. In the study, TBL is calculated for rough surfaces by using modified eddy viscosity model of Cebeci and Smith. Also, they extended the study of Cebeci and Keller to consider the roughness effect with and

without a pressure gradient. Compared to the method of Bradshaw et al. [17] (in which the transport equation approach of differential method is used), one fewer equation was solved. In addition, Keller Box scheme [15], which allows proper and economical solutions to differential equations, was used.

In order to take the effect of the surface roughness into consideration, modifications to the near-wall approach were applied to the eddy viscosity model of Cebeci and Smith which is based on Rotta's method [16]. For modified eddy-viscosity, the mixing length was changed to reflect the roughness effect to the TBL calculation.

The method is valid for $4.535 < k_s^+ < 2000$, where the upper limit corresponds to Rotta's displaced model and the lower limit corresponds to the upper bound of the hydraulically smooth surface. In addition, in the cases where the k_s is not provided, Dvorak's correlation [12] within the range of applicability can be used to obtain the k_s value.

The method was used for a limited roughness geometry and limited pressure gradient value. Nevertheless, the model provides enough precision according to the comparison with respect to the experimental results, at least for the design purposes [16].

In the differential method of Bradshaw et al. [17], the transport equation approach is employed. Turbulence energy equation (TEE) with some assumptions was utilized which allows the hyperbolic equations to be solved.

Generally, numerical studies are based on "Mixing length" or the "eddy-viscosity" assumption. According to the assuming, the shear stress at any station related to the mean-velocity gradient at this station [18]. However, according to Bradshaw and Ferriss [19] turbulent (or Reynolds) stress, $-\rho\overline{uv}$, is rather related to the turbulent kinetic energy (TKE) which is governed by TEE. In addition, the connection between the mean-flow and the shear stress profile is not valid for the boundary layers with a pressure gradient. This is because the solution method of Navier-Stokes equations is a result of the parabolic equation system [17].

If the relationship between the intensity, dissipation, diffusion and the shear stress terms is known, the TKE equation can be converted into an equation which is responsible for the rate of change of turbulent shear stress, $-\rho\overline{uv}$. The mean continuity equation, the mean momentum equation and the converted form of TKE create a hyperbolic system together [17]. Any hyperbolic system can be solved with ease by characteristics method.

According to the experimental study of Antonia and Wood [20], calculation of TBL, in which method of Bradshaw and et al. is used, gives satisfactory results for d-type roughness. Another study is conducted by Antonia and Luxton [21]. As a result of their study; for the larger roughness changes, such as k-type roughness, separation from the equilibrium-layer is significant. Therefore, a different equation for the length scale of the modified turbulence field should be used.

Another important classification in the literature is how CFD tools represent the effect of surface roughness on the numerical calculations of TBL.

Today, plenty of engineering tools depend on "wall similarity theory of Townsend" to represent the roughness effect on the flow. According to the wall similarity theory, influence of roughness effect on the surface is imprisoned in the inner layer (Figure 1.4) and, overlap and outer part of the boundary layer is not affected from the surface roughness. The assumption behind the theory is that the TBL thickness is relatively high compared to the roughness element height. As a result of this approach, an important practical solution is achieved for TBL calculation both numerically and analytically [22].

Hama [23] pointed out that the velocity-defect law in zero pressure gradient flow, that is used to define velocity distribution over wall-bounded turbulent flow, is not affected by roughness. With the light of such finding, Clauser [24] and Rotta [25] introduced roughness function, ΔU^+. According to Clauser and Rotta's studies, the fundamental effect of roughness is the shift in the mean velocity profile in the logarithmic-law. Shifting downward is represented by ΔU^+.

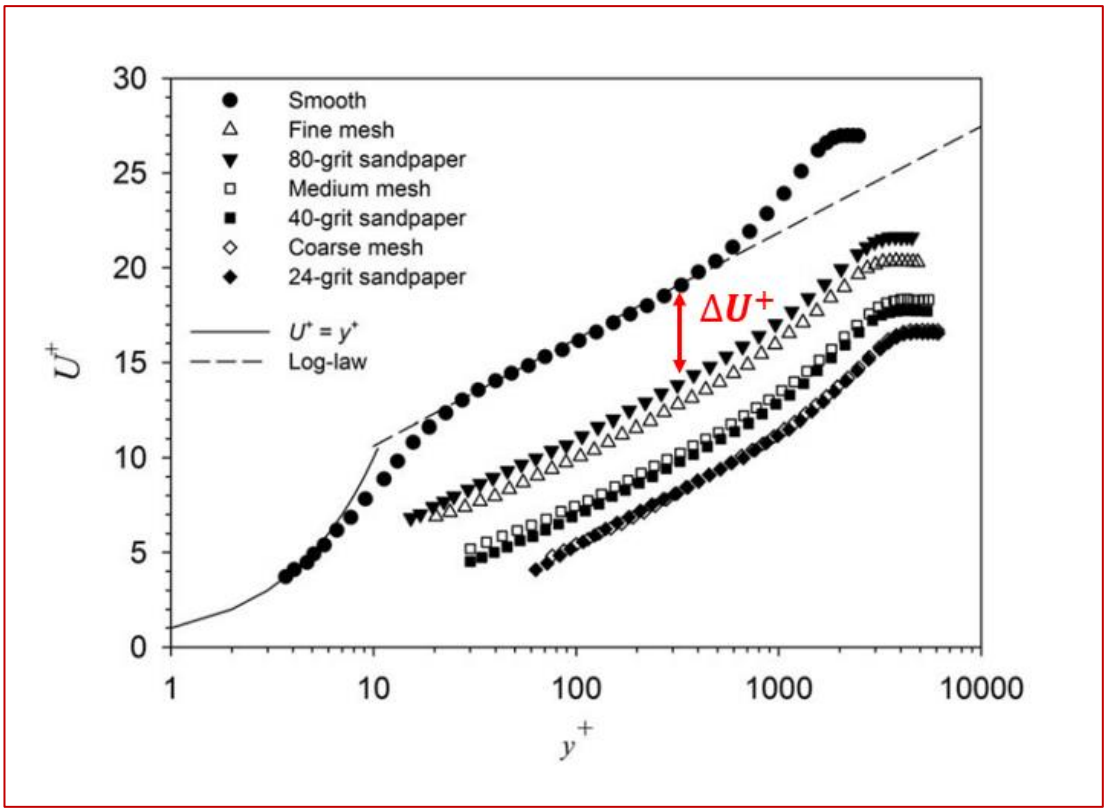

Figure 1.5 Roughness function for mesh and sand grain roughness [22]

Eqn. (1.21) is the velocity distribution for TF and ΔU^+ represents the effect of roughness.

$$U^+ = \frac{1}{\kappa}\ln y^+ + A - \Delta U^+ + \frac{2\varpi}{\kappa}W\left(\frac{y}{\delta}\right) \tag{1.21}$$

where;

U^+ : nondimensional velocity distribution,

κ : von Kármán constant,

y^+ : nondimensional wall distance perpendicular to solid boundary,

A : smooth wall intercept constant that represents the effect of geometric boundaries shape and length on the velocity distribution,

ΔU^+ : roughness function,

ϖ : wake parameter,

W : wake function,

δ : TBL thickness,

y : spatial coordinate for wall normal direction in cartesian coordinate system.

In the velocity distribution equation, Eqn. (1.21), there are terms named wake parameter and wake function. The latter one represents the deviation of the outer layer profile from the logarithmic-law, Figure 1.4, and according to the experiments, its character is universal. By performing an empirical fit to the measured velocity profile, it is obtained as $1 - cos(\pi y/\delta)$ [15]. For the all cases, $W(1)$ is equal 2, hence W is the normalized shape function and its variation in the flow direction is represented by the wake parameter, ϖ.

As an example; CFD solvers, such as Star-CCM+ and ANSYS Fluent, calculate the drag force based on roughness function (ΔU^+) approach. To consider the roughness effect, k_s should be determined. For a uniform sand-grain roughness, value of k_s can be taken as the height of the sand-grain (diameter of the sand-grain). For the other types of roughness, equivalent sand-grain roughness could be used by a correction factor, C_s, and its value depends on the type of the roughness given.

Although calculating TF over a rough surface with the help of roughness function is a practical way and it is used by a number of CFD tools, defining a proper roughness function is not easy. Because there is no universal ΔU^+ and it is a function of roughness geometry, size and density [12]. Hence, a number of studies in the literature are focused on obtaining more general roughness function. Therefore; while obtaining ΔU^+, less assumptions can be done and accordingly more realistic TBL solutions can be achieved by CFD tools.

1.5 Outline of the Thesis

The literature survey, given in Section 1.4, summarizes the former methods to obtain the skin-friction coefficient. Schlichting skin-friction formula is discussed by introducing the physic of the flow. Moreover, some studies related to the numerical

calculation of rough TBL with and without pressure gradient are summed up with respect to the solution method (integral or differential). Finally, how today's CFD tools represent the effect of surface roughness on the numerical calculations of TBL is introduced.

The mathematical model used throughout the numerical solution of TBL are obtained and presented in CHAPTER 2. Solution technique to calculate the TBL parameters for the present work is submitted. The flow diagram for the developed code is shared. Eventually, the convergence of solution and grid independence studies (which are performed to be sure that the results of the developed code are independent of the discretization used in the numerical implementation and the solution converges) are presented.

In CHAPTER 3, comparison of the present study is done with the help of experimental studies, Cebeci and Chang's numerical study [16] and Schlichting skin-friction formula [4].

Discussions related to the results of the present study are carried out in CHAPTER 4. The success of the solution technique (which considers the relative size of the thicknesses of the sublayers and the roughness height with respect to each other, and in which the fluid mechanics equations conjugation with Nikuradse's experiment results) is emphasized. Finally, ideas for the future work and the expectations based on them are given.

CHAPTER 2

MATHEMATICAL MODEL AND CALCULATION METHOD

The main idea behind the calculation of TBL for the present study is; if all TBL parameters are known at a solution-point (SP-1), it is possible to obtain the δ_2 for the next solution-point (SP-2) by using the momentum integral equation. Furthermore, if the velocity distribution is known for the SP-2, it is also possible to find the TBL parameters which belong to the SP-2 as well. Therefore, their equality gives rise to an equation to find the unknown parameter used to formulate the velocity distribution. In our case this is C_f.

To obtain the velocity distribution for SP-2; knowing A', C_f, ϖ are necessary. By using the relationship between C_f and δ, and assuming the C_f value for the SP-2, the velocity distribution for the SP-2 can be achieved.

This logic works for all kind of two-dimensional TF over a rough surface. In the present study, its special condition which is flow with zero pressure gradient is examined.

2.1 Mathematical Model

In the present study, mainly five fluid mechanics equations are used which are given as in the following:

i. The momentum integral equation,
ii. Velocity distribution for whole turbulent boundary layer thickness,

iii. Rough wall intercept constant, A', variation according to Nikuradse's sand roughness experiments [4],
iv. Momentum thickness equation,
v. Non-dimensional local skin-friction coefficient equation.

In order to use the equations above more coordinately in the calculation steps of the present study, they should be simplified and converted into useful forms. After the conversion process, the solution technique of the present study is clarified in Section 2.2.

2.1.1 Momentum Integral Equation

For two-dimensional incompressible TBLs, the momentum integral equation is defined as in the Eqn. (1.10). Under the condition of zero pressure gradient; the $d\overline{U}_E/dx$ term in the Eqn. (1.10) goes to zero inherently. Hence it is converted into the form:

$$\frac{d\delta_2}{dx} = \frac{C_f}{2} \tag{2.1}$$

To obtain δ_2 for any solution-points (SPs), first order finite difference approximation which is presented in Eqn. (2.2) is used.

$$\delta_2\left(x+\Delta x\right) = \delta_2\left(x\right) + \Delta x \left.\frac{d\delta_2}{dx}\right|_x \tag{2.2}$$

By substituting Eqn. (2.1) into Eqn. (2.2), the formulation which gives the momentum thickness for any SP is obtained.

$$\delta_2\left(x+\Delta x\right) = \delta_2\left(x\right) + \Delta x \left.\frac{C_f}{2}\right|_x \tag{2.3}$$

2.1.2 Velocity Distribution Equation

For a TF over a rough surface, velocity distribution can be written as:

$$U^{+} = A' + B\ln\frac{y}{k_s} + \frac{\varpi}{\kappa}W\left(\frac{y}{\delta}\right) \tag{2.4}$$

where;

A' : rough wall intercept constant that represents the effect of geometric boundaries shape and length on the velocity distribution.

When the boundary condition "$y = \delta \rightarrow \bar{U}(y) = \bar{U}_E$" is applied to the velocity distribution, Eqn. (2.4), the following equation can be obtained.

$$\frac{\bar{U}_E}{U_\tau} = A' + B\ln\frac{\delta}{k_s} + 2B\varpi \tag{2.5}$$

Another form of the velocity distribution (named velocity-defect law) is also used in the calculation steps of the present study. Subtracting Eqn. (2.5) from the velocity distribution, Eqn. (2.4), the velocity-defect law can be obtained as:

$$\frac{\bar{U}_E - \bar{U}}{U_\tau} = f\left(\frac{y}{\delta}\right) = -B\left\{\ln\left(\frac{y}{\delta}\right) + \varpi\left[W\left(\frac{y}{\delta}\right) - 2\right]\right\} \tag{2.6}$$

where;

f : velocity-defect law which is a function to be determined by experiments [2].

At-large Re, the velocity-defect law takes universal form. Especially in the flow over a flat plate in the zero pressure gradient, it is not affected by surfaces roughness and therefore is independent of Re [26].

One explanation of velocity-defect law's independence from surface roughness may be done by considering the constant shear layer concept, the mixing length theory and the energy spectrum of a TF.

(a) Constant Shear Layer

In most wall-bounded TF, there is a region adjacent to the wall in which total shear stress is approximately constant. This region is named constant-shear-stress layer and composed of three main regions named; viscous sublayer, buffer layer and fully turbulent layer [7].

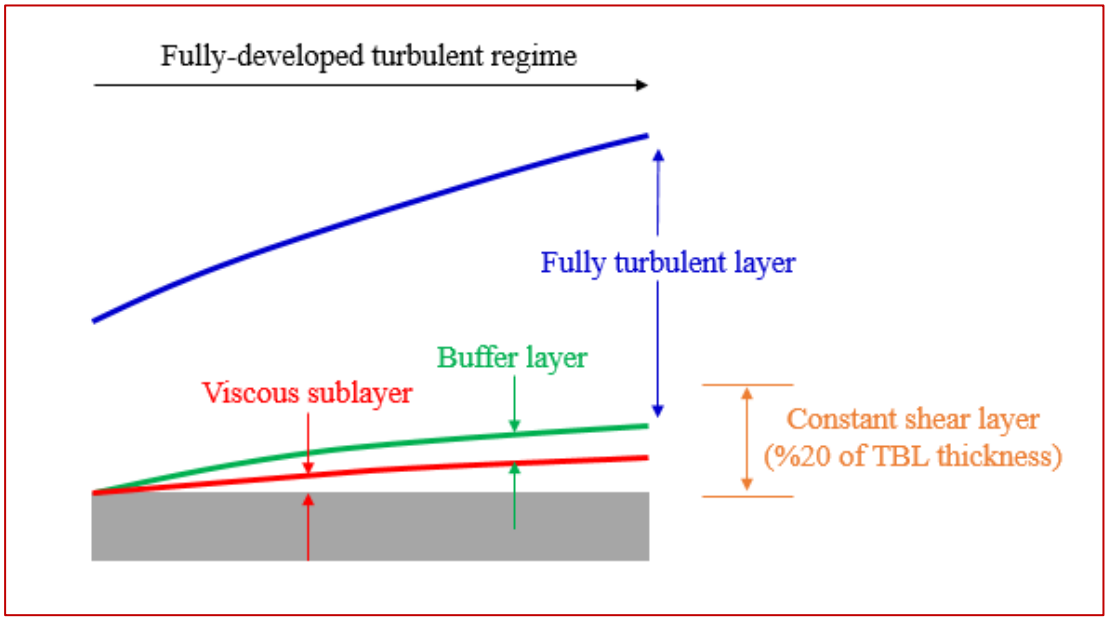

Figure 2.1 Constant shear layer in TBL (schematic)

Therefore, in the constant shear layer, the total shear can be considered as:

$$\begin{aligned} \tau_{tot} &= \tau_W = \tau_V && \text{in the viscous sublayer} \\ \tau_{tot} &= \tau_W = \tau_V + \tau_T && \text{in the buffer layer} \\ \tau_{tot} &= \tau_W = \tau_T && \text{in the fully turbulent layer} \end{aligned} \tag{2.7}$$

where;

τ_{tot} : total shear stress,

τ_w : wall shear stress,

τ_v : viscous shear stress,

τ_T : turbulence shear stress.

(b) Turbulent Mixing Length Theory

In the derivation process of the momentum integral equation, terms in mean continuity and mean momentum equations (RANS) for a TF of incompressible fluids are multiplied by "dy" elementary length and taken the integral from 0 to ∞ [3]. In the RANS equation (for TFs of incompressible fluids), there is an additional term named turbulence stress, unlike the RANS equation of laminar flows. This term is responsible for the extra the momentum flux between TBL sublayers.

Defining turbulence stress in terms of flow parameters is impossible at least for today. Because, there are ten unknowns and only four equations to obtain the TF's parameters. This situation is named "Turbulence Flow Closure Problem". To overcome this problem, turbulence modeling concept is used.

Mixing length theory assumes that a mass of fluid maintains its identity over a certain distance after which it loses its momentum to the neighborhood environment and naturalizes the properties of its surrounding [27].

Prandtl defined it as [4]:

$$\tau_T = \rho l_m^{\,2} \left|\frac{d\overline{U}}{dy}\right| \frac{d\overline{U}}{dy} \tag{2.8}$$

where;

l_m : mixing length.

In a flat wall-bounded flow, mixing length is described as:

$$l_m = \kappa y \tag{2.9}$$

where;

κ : von Kármán constant,

y : perpendicular distance between the solid boundary and any point in the boundary layer.

(c) Energy Spectrum of Turbulent Flow

In the energy spectrum (Figure 2.2), there are mainly three regions. The fr_E represents the wave number which corresponds to the maximum energy, whereas the fr_D stands for the wave number that corresponds to the minimum energy in the spectrum.

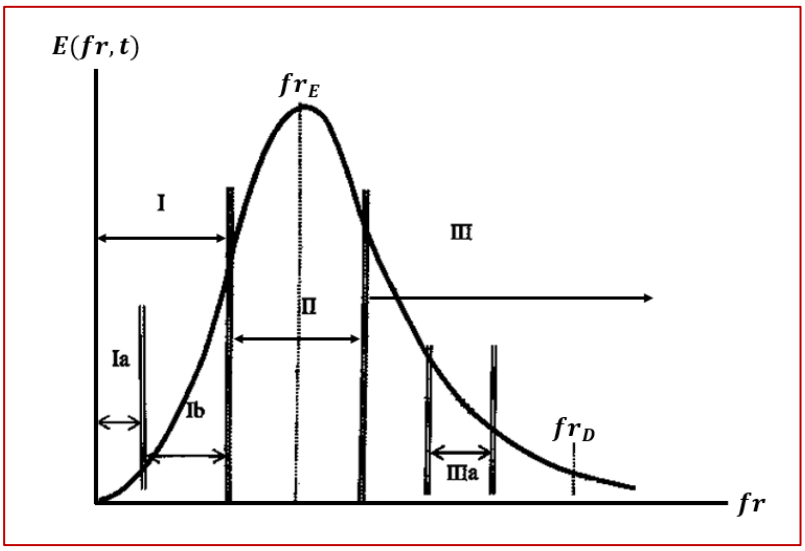

Figure 2.2 Three-dimensional energy spectrum with critical regions [7]

The first region in Figure 2.2 represents the large eddies, which are responsible for the chaotic structure of a TF. Hence, the region is called “Largest eddies region” and the solid boundaries are the source for the large eddies in TF. Briefly, eddies are related to geometric boundaries shape and length.

The second region, the individual energy dissipation of the eddies is lower compared to the energy dissipation in the first region. Hence, the energy intensity in the second region reaches its maximum value. Therefore, the region is named “Energetics eddies region”.

The third region extends from fr_E to fr_D. In the case of Re is large enough, that is ($fr_E \ll fr_D$), and if the viscous dissipation can be neglected, the total energy of the eddies in the TF maintains a constant value. Therefore, the eddies in the third regime are in the "equilibrium state" in terms of statistical, and they gradually become independent from the effect of the large eddies. Hence, eddies between $fr_E - fr_D$ range are independent from the boundary conditions (such as surface roughness). Since such physical mechanism is universal, the third region is named "Universal equilibrium range" (UER).

To obtain the velocity-defect law for wall-bounded TF (in which Re is high) the mixing length theory is used. The characteristics of the approach adopted in TML derivation is very similar to the UER in the energy spectrum. Therefore, it can be said that TML theory represents the UER. One of the most significant characteristics of the UER is the motion of fluid particles are independent of the direct wall effect. Consequently, independence of the velocity-defect formulation from surface roughness is an expected result.

On the other hand, if Re is not large enough to use velocity-defect law, laminar-friction exerts some of its effects outside the thin sublayer (sum of viscous sublayer and buffer layer) [4]. Hence, the validity of logarithmic-law and accordingly velocity-defect law loses its applicability.

2.1.3 Rough Wall Intercept Constant, A', Determination

In the velocity distribution equation, Eqn. (2.4), there is a term named rough wall intercept constant, A'. It represents the effect of the large eddies in a TF. Because solid boundaries are source for large eddies, values of A' related to geometric boundaries shape and length. Whereas its value is 5.5 for a smooth surface, it changes between 8.5 and 9.5 for a rough surface in a TF over a flat plate with zero pressure gradient [7].

Nikuradse used equivalent sand grains in his pipe experiments to generate a roughness on a surface. Thus, he was able to express the effect of the roughness on the fluid flow

by using the equivalent sand roughness height, k_s. It is defined as diameter of sand grains, and a surface spreaded with these closely packed sand grains creates the same drag effect with surface roughness interested. Hence, the variation of A' was graphed as a function of k_s by Nikuradse, as presented in Figure 2.3.

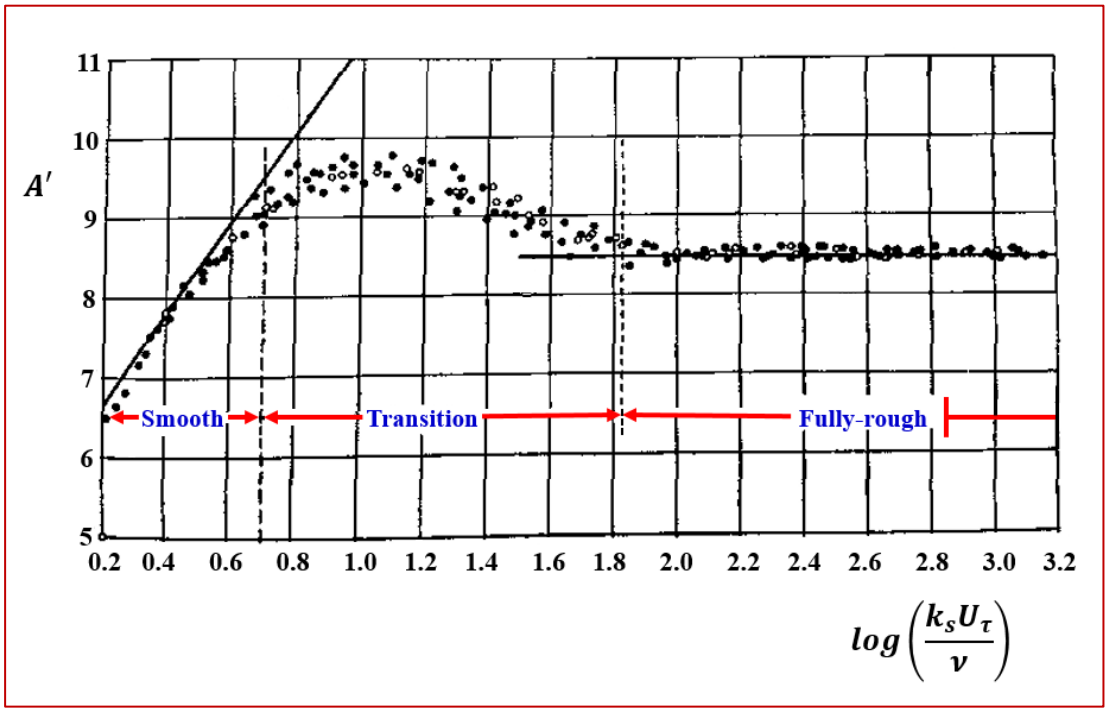

Figure 2.3 A' variation in terms of $k_s U_\tau/\nu$ for Nikuradse's sand roughness [4]

For the k_s^+ variation according to Nikuradse's sand roughness experimental results (Figure 2.3), Yalın and Da Silva's [28] correlation is employed. The correlation is given as:

$$A' = +\left(2.5\ln k_s^+ + 5.5\right)\exp\left[-0.0705\left(\ln k_s^+\right)^{2.55}\right] + 8.5\left\{1-\exp\left[-0.0594\left(\ln k_s^+\right)^{2.55}\right]\right\} \tag{2.10}$$

where;

k_s^+ : nondimensional equivalent surface roughness, $k_s U_\tau/\nu$.

2.1.4 Momentum Thickness Equation

Momentum thickness can be derived by considering the loss of momentum compared to potential flow in a 2D TBL for incompressible fluids, and it is defined as:

$$\delta_2 = \int_0^{\infty} \frac{\overline{U}(y)}{\overline{U}_E}\left(1-\frac{\overline{U}(y)}{\overline{U}_E}\right)dy \tag{2.11}$$

where;

$\overline{U}(y)$: velocity distribution of TBL in perpendicular direction to the solid boundary.

By multiplying and dividing the Eqn. (2.11) with friction-velocity (U_τ), introducing $y/\delta = \eta$ and using the velocity-defect law, Eqn. (2.6), the following form of momentum thickness equation can be achieved:

$$\frac{\delta_2}{\delta} = C_1\frac{U_\tau}{\overline{U}_E} - C_2\left(\frac{U_\tau}{\overline{U}_E}\right)^2 \tag{2.12}$$

Having combined the Eqn. (2.12) and Eqn. (2.5), the momentum thickness equation is converted into the form:

$$\delta_2 = \delta\left\{C_1\left[\frac{1}{A'+B\ln\left(\delta/k_s\right)+2\varpi B}\right] - C_2\left[\frac{1}{A'+B\ln\left(\delta/k_s\right)+2\varpi B}\right]^2\right\} \tag{2.13}$$

where;

$$C_1 = \int_0^1 f(\eta)\,d(\eta)$$
$$C_2 = \int_0^1 f^2(\eta)\,d(\eta) \tag{2.14}$$

C_1 and C_2 values used by different researchers are presented in Table 2.1. Considering the value of C_1 and C_2 as a constant may give satisfactory results in the calculation of

a rough TBL parameters. However, better results may be obtained by calculating the values of C_1 and C_2 at every solution-point (SP) on the calculation domain. Since the velocity-defect law is a function of ϖ and δ, C_1 and C_2 are also functions of them. Thus, it is necessary to compute C_1 and C_2 at every SP on the solution domain and which are calculated in such manner in the present study.

Table 2.1 Different values of $\boldsymbol{C_1}$and $\boldsymbol{C_2}$ expressed by three different researchers

	C_1	C_2
Clauser [24]	3.6	22
Schulz-Grunow [29]	3.34	-
Coles [30]	4.05	29

2.1.5 Skin-Friction Coefficient Equation

Nondimensional local skin-friction coefficient is defined as:

$$C_f = \frac{2\tau_w}{\rho\left(\overline{U}_E\right)^2} \tag{2.15}$$

where;

τ_w : wall shear stress,

ρ : density of the fluid.

By substituting ρU_τ into the τ_w in Eqn. (2.15), the following equation can be obtained:

$$\frac{\overline{U}_E}{U_\tau} = \left(\frac{2}{C_f}\right)^{1/2} \tag{2.16}$$

By means of Eqn. (2.5), skin-friction coefficient can be written as:

$$C_f = \frac{2}{\left(A' + B \ln \frac{\delta}{k_s} + 2B\varpi \right)^2} \tag{2.17}$$

2.2 Solution Technique

In the computational domain, in Figure 2.4, any points in the fully-developed turbulent regime can be selected as a starting point for the TBL calculation in the present study. Throughout the calculation process, forward marching method, which calculates the TBL parameters step by step, is employed. The method allows the determination of parameters at solution-point-2 (SP-2) by knowing initial conditions at solution-point-1 (SP-1). Then, parameters can be calculated at SP-3 by using the obtained values of SP-2. The procedure is repeated for the all SPs in a chosen computation domain. At the end of the calculation, TBL thickness, displacement thickness, momentum thickness and skin-friction coefficient, which are called TBL parameters, are obtained for all SPs.

For the present study, it is essential and enough to know the initial values of:

a. the wake parameter, ϖ,
b. the local skin-friction coefficient, C_f,
c. the momentum thickness, δ_2,

at a starting point, SP-1 in Figure 2.4. In addition, the flow parameters, such as free-stream velocity, U_E, fluid viscosity, μ, and the flat plate features, such as equivalent sand roughness height, k_s, have to be known.

Steps followed throughout the numerical calculation of TBL are itemized below:

i. The calculation process starts at the SP-1, in Figure 2.4. By using the initial value of ϖ and the Eqn. (2.14), both C_1, and C_2 constants are obtained for the SP-2,

ii. For the next solution-point (SP-2), the momentum thickness, δ_2, is obtained by using the Eqn. (2.3),

iii. By using the initial value of the C_f, and by means of the Eqn. (2.16), k_s^+ value and the Eqn. (2.10), A' is acquired,

iv. The TBL thickness, δ, (of which calculation depends on the Newton-Raphson method since Eqn. (2.13) presents an implicit equation) is calculated by using the Eqn. (2.13).

All the obtained values except for the δ_2 are the estimated values for the SP-2. Because in step (ii), the value of A' is obtained by using the C_f value at the SP-1. However, its value depends on the C_f value at the SP-2. Hence, before proceeding to calculate the TBL parameters for the SP-3, values at the SP-2 should be checked whether they are correct or not. For this purpose:

v. The Eqn. (2.17) is used to check whether the obtained C_f value for SP-2 is correct or not. If not, as far as the C_f value converges, steps i, ii, iii and iv are repeated.

The convergence criterion for C_f values and accordingly for the other TBL parameters is that; for a SP, if the absolute percentage change between the obtained C_f values in consecutive iterations is lower than the value of 1, its value which is obtained in the last iteration is considered as the correct value.

At the end of the step (v), TBL parameters at the SP-2 are achieved by using the ϖ value at the SP-1, and throughout the calculation between the SP-1 and the SP-2, the

value of ϖ does not change (and accordingly the values of the terms in which ϖ is used to the compute them). However, for a given free-stream velocity, the ϖ is a function of the C_f, δ and k_s according to the Eqn. (2.17). From this point of view, the value of ϖ should change at the SP-2. Therefore, the calculated TBL parameters at the SP-2 are still not the exact values.

To overcome such complication, it was in searched of a different method to achieve a correct value of ϖ at SP-2, and after having obtained its accurate value, it can be used to obtain the exact values of TBL parameters at SP-2.

In the present study, wake parameter is computed and embedded in the relevant equations at every SP on the calculation domain by using a method developed during this study. The method used a relationship between C_f and ϖ values which is tested with the experimental works in the literature. The relationship can be summarized as:

$$\varpi_{SP(n)} \propto \frac{C_{f\_SP(n)}}{C_{f\_SP(n-1)}} \varpi_{SP(n-1)} \tag{2.18}$$

where;

$\varpi_{SP(n)}$: ϖ value at SP-n,

$\varpi_{SP(n-1)}$: ϖ value at SP-(n-1),

$C_{f\_SP(n)}$: C_f value at interested SP-n,

$C_{f\_SP(n-1)}$: C_f value at the previous interested SP-(n-1) (with respect to Figure 2.4).

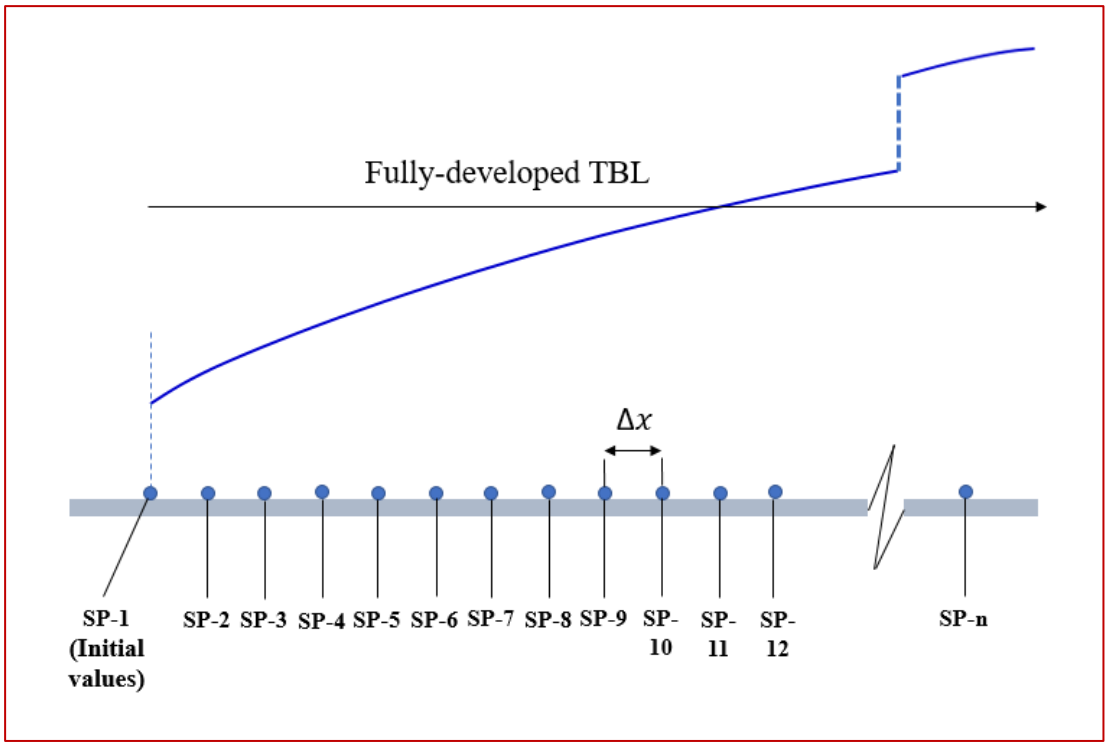

Figure 2.4 Solution-points (SPs) and the distance between them (Δx) in the present study

It is also noticed that the ϖ is not needed to be calculated at every SP throughout the flat plate, and its frequency can be larger than the distance between two consecutive SPs (Δx) (such as the distance between SP-5 and SP-6 or SP-n and SP-(n-1)). Therefore, time consumption for the calculation of TBL parameters can be decreased.

On the other hand, since one of the main purposes of the present study is calculating the mean skin-friction coefficient (C_D), the frequency of the points in which ϖ is computed is important. This is due to the fact that the more computed wake parameter values used, the more accurate the C_f values, and accordingly, the C_D value are going to be obtained for a flat plate. Hence, in Section 2.4, the grid independence study of the present work is performed, and the optimal value for the frequency of points in which ϖ computed is clarified.

In the light of the explanations above, the last step for the calculation of TBL parameters at SP-2 is:

vi. After having converged C_f value at SP-2, a proper ϖ value for SP-2 is obtained by using the Eqn. (2.18) and repeating the steps i, ii, iii, iv, v three times. At the end of the last repetition, the TBL parameters exact values for the SP-2 are achieved.

For the solution of TBL, the calculation steps (i, ii, iii, vi, v, vi, vii) are reflected for the all SPs in a chosen computation domain.

Moreover; if the displacement thickness (δ_1) wished to be calculated, the Eqn. (2.20) should be used, which is obtained by substituting the Eqn. (2.5) into the displacement thickness equation, Eqn. (2.19).

$$\delta_1 = \int_0^{\infty} \left(1 - \frac{\overline{U}(y)}{\overline{U}_E} \right) dy \tag{2.19}$$

$$\delta_1 = \delta \left\{ C_1 \left[\frac{1}{A' + B \ln\left(\delta / k_s\right) + 2\varpi B} \right] \right\} \tag{2.20}$$

Flow diagram of the developed code which performs such calculation procedure is presented in Figure 2.5.

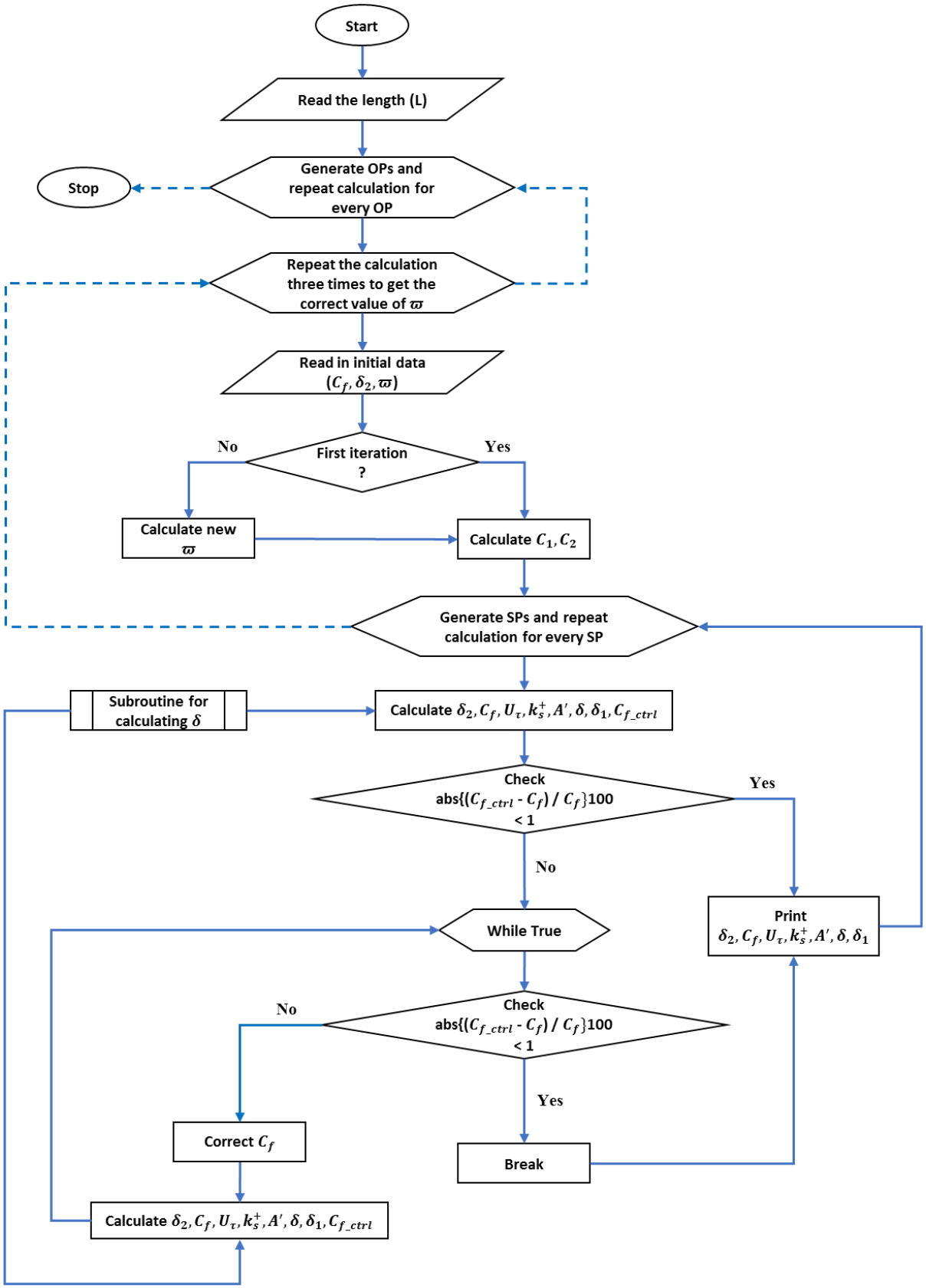

Figure 2.5 Flow diagram of the developed code

2.3 Convergence of Solution Study

In the present study, numerical calculation of TBL parameters is an iterative process, which is one of the numerical solution methods. At the end of an iterative calculation, the method may lead to a solution or lead away from solution. If the method leads to a solution, then it is said that the method is convergent. Otherwise, the method is said to be divergent.

In the present study, the C_f and the remaining TBL parameters are obtained by using a system of equations mentioned in CHAPTER 2. One of them is the Eqn. (2.17), and it is used to check the accuracy (or convergence) of obtained C_f value at a SP.

In Figure 2.6, the convergence of C_f value at an arbitrary SP is presented. Until the convergence of C_f values are to be ensured with respect to the convergence criterion for the present study (mentioned in Section 2.2), the new C_f values are acquired for this SP.

Because of the convergence criterion algorithm in the developed code, similar results are obtained for the all SPs throughout a calculation process. Therefore, it can be said that the convergence of the solution to obtain the TBL parameters is achieved.

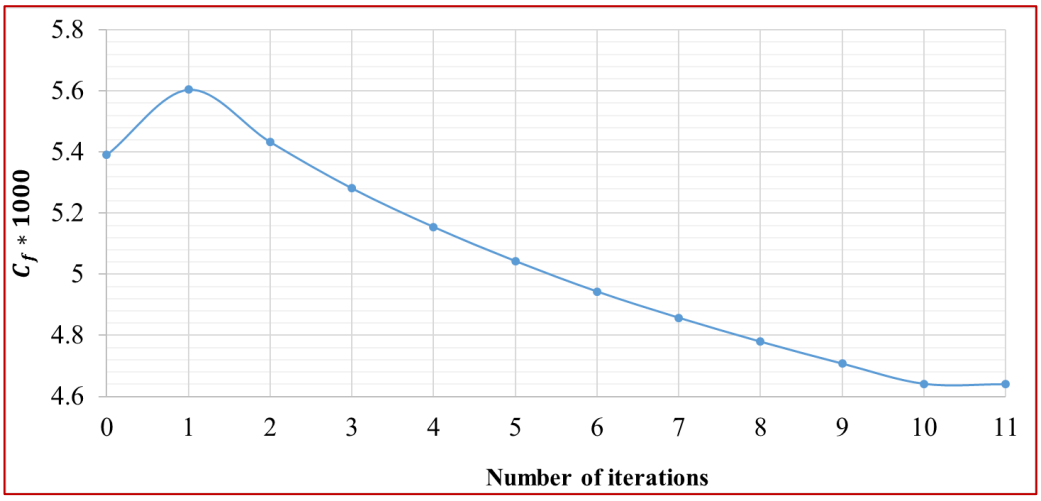

Figure 2.6 C_f variation with respect to number of iterations at an arbitrary SP

2.4 Grid Independence Study

To obtain a numerical solution of a fluid flow, any geometry in any dimensions need to be discretized. The result of the discretized fluid flow domain is named as the solution grid.

In the derivation process of the momentum integral equation, Eqn. (1.10), terms in mean continuity and mean momentum equations (RANS) are multiplied by "dy" elementary length and taken the integral from 0 to ∞ [3]. Because the integration operation is performed in the y-direction, the equations' dependency to "y" disappears. Hence, the final equation is an ordinary differential equation and its dependency is only in the flow direction, that is x-direction (Figure 2.7) in the present study. Hence, it is appropriate to generate a one-dimensional grid only in the x-direction.

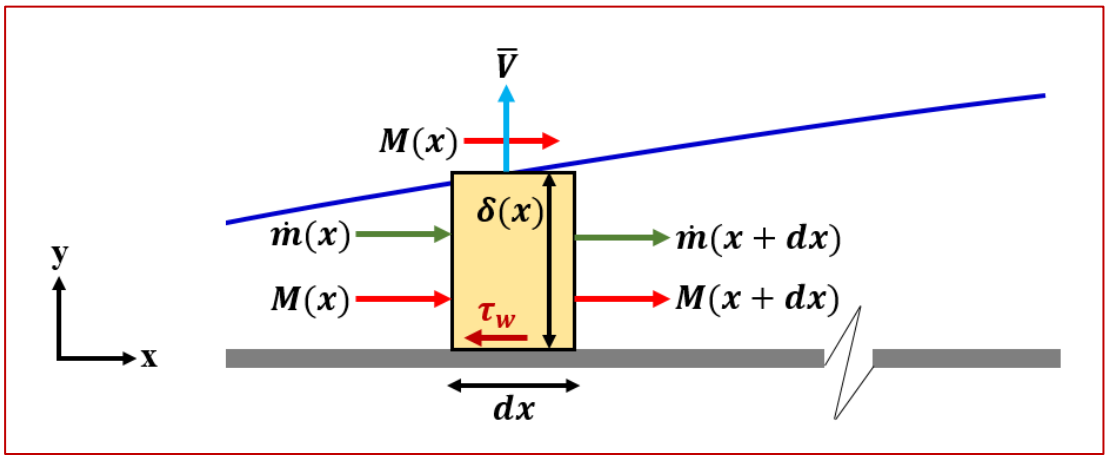

Figure 2.7 Obtaining momentum integral equation [3]; the M is momentum, the $\dot{m}$ is mass flow and the $\bar{V}$ is velocity component in y-direction

For the grid independence study (GIS), different grids lengths (or the different number of SPs) are used. However, electronic numerical calculator's (ENC) memory requirement increases as the number of SPs is increased. Hence, reduction of SPs is a necessity for the memory consumption of ENC. On the other hand, decreasing the

number of SPs can cause degradation in solution precision. Hence, while reducing the number of SPs, the results should be conserved. Therefore, the grid should include the lowest number of elements, while not affecting the results in the solution domain.

In the calculation domain, there are mainly two types of points (as presented in Figure 2.8), on which the calculation of TBL parameters performed. The blue ones are named solution-point (SP), and the red ones are named output-point (OP). In other words, some specific OP is named SP. At the SPs, except for the wake parameter value (ϖ), all TBL parameters are calculated. On the other hand, at the OPs, all TBL parameters are computed. Therefore, GIS is performed for both the SPs and the OPs.

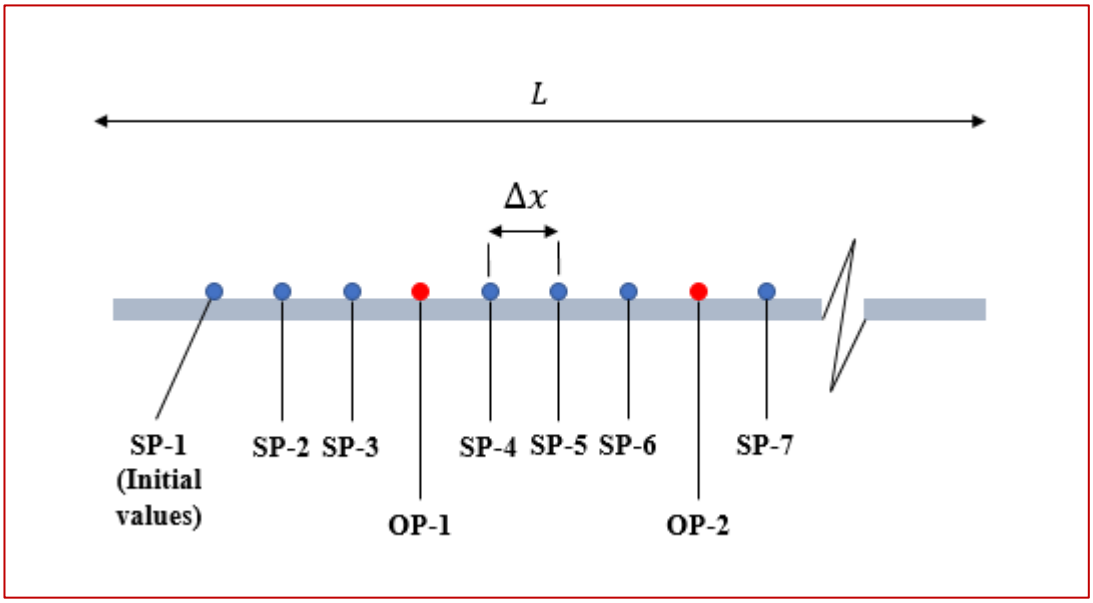

Figure 2.8 Grid length (Δx), solution-points (SPs), output-points (OPs), length of the plate's portion interested in fully-turbulent flow (L)

During the GIS, a workstation with Intel(R) Core(TM) i7 CPU M620 @ 2.67Ghz core and 4GB RAM is used.

2.4.1 Grid Independence Study for the Solution-Points

In the present study, the GIS is performed by using different grid lengths, Δx, which is defined as the distance between two consecutive SPs (such as the distance between SP-4 and SP-5) on the calculation domain shown in Figure 2.8. The C_f is calculated for the different $L/\Delta x_{SP}$ values which equal to 2, 4, 8, 20, 40, 200, 400, 2000, 4000, 20000 and 40000 respectively.

The C_f variation with respect to the different $L/\Delta x_{SP}$ values is drawn and presented in Figure 2.9. Furthermore, the results and the calculation times for the different $L/\Delta x_{SP}$ values are submitted as a table in Table 2.2.

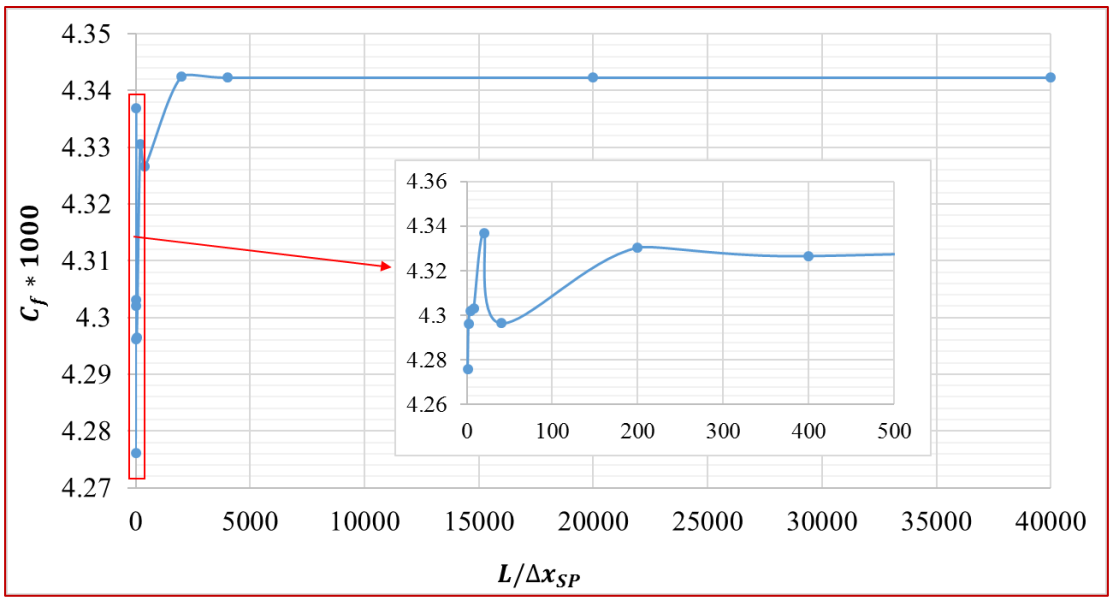

Figure 2.9 C_f variation with respect to the different $L/\Delta x_{SP}$ values

According to Figure 2.9; grid independence is achieved when the $L/\Delta x_{SP}$ value equals to 4000. However, it should be noted that the higher the number of SPs (or higher value of $L/\Delta x_{SP}$) is the higher the requirement for ENC memory. It is inferred from Table 2.3 that by accepting the < 0.13% error, the $L/\Delta x_{SP}$ value which equals 20 can

be used instead of using the $L/\Delta x_{SP}$ value which equals 4000. Therefore, the computation time is reduced approximately 78 times, which is tremendous. Results of such evaluations are presented in Table 2.3. In the table, the relationship between the errors and the computational time reductions with respect to the grid independent $L/\Delta x_{SP}$ value which equals 4000 can be found.

Table 2.2 Local skin-friction coefficient (C_f) values at the end of the plate for the different $L/\Delta x_{SP}$ values

Δx [mm]	$L/\Delta x_{SP}$	C_f value at 2 m	Calculation time [s]
1000	2	0.004296192	0.6
500	4	0.004302095	1.1
250	8	0.004303036	2.2
100	20	0.004336861	4.2
50	40	0.00429647	7.4
10	200	0.004330485	19.4
5	400	0.004326677	41.6
1	2000	0.004342475	147.1
0.5	4000	0.004342305	329.0
0.1	20000	0.004342305	1165.8
0.05	40000	0.004342305	2820.3

Table 2.3 The computation time reductions and the errors for the different $L/\Delta x_{SP}$ values with respect to (wrt) its grid independent value (4000)

Δx [mm]	$L/\Delta x_{SP}$	Calculation time [s]	Error wrt $L/\Delta x_{SP}$ value of 4000 [%]	Calc. time reduction wrt $L/\Delta x_{SP}$ value of 4000 [times]
1000	2	0.6	1.073	583.9
500	4	1.1	0.935	289.9
250	8	2.2	0.913	150.2
100	20	4.2	0.126	78.3
50	40	7.4	1.067	44.5
10	200	19.4	0.273	16.9
5	400	41.6	0.361	7.9
1	2000	147.1	-0.004	2.2
0.5	4000	329.0	0.000	1.0
0.1	20000	1165.8	0.000	0.3
0.05	40000	2820.3	0.000	0.1

2.4.2 Grid Independence Study for the Output-Points

For the GIS of OPs, $L/\Delta x_{SP}$ value is taken as constant and only the value of $L/\Delta x_{OP}$ is changed. It should be noted that the distance between the two OPs should be equal to or more than the distance between two SPs, the contrary is not meaningful. Hence, the minimum distance between two OPs should be the same with the distance between the two SPs, Δx. The C_f is calculated for the different $L/\Delta x_{OP}$ values which equal to 2, 4, 8, 20, 40, 80, 200 respectively.

The C_f variation with respect to the different $L/\Delta x_{OP}$ values is drawn and presented in Figure 2.10 Furthermore, the results and the calculation times for the different of $L/\Delta x_{OP}$ values are submitted as a table in Table 2.4.

According to Figure 2.10, grid independence is achieved when the $L/\Delta x_{SP}$ value equals to 200. However, it is inferred from Table 2.5 that by accepting < 0.5% error, the $L/\Delta x_{SP}$ value of 20 may be used instead of 200. Therefore, computation time can be reduced approximately 90.5 times, which is tremendous. The relationship between the errors and time reductions with respect to the grid independent $L/\Delta x_{SP}$ value which equals 200 can be found in Table 2.5.

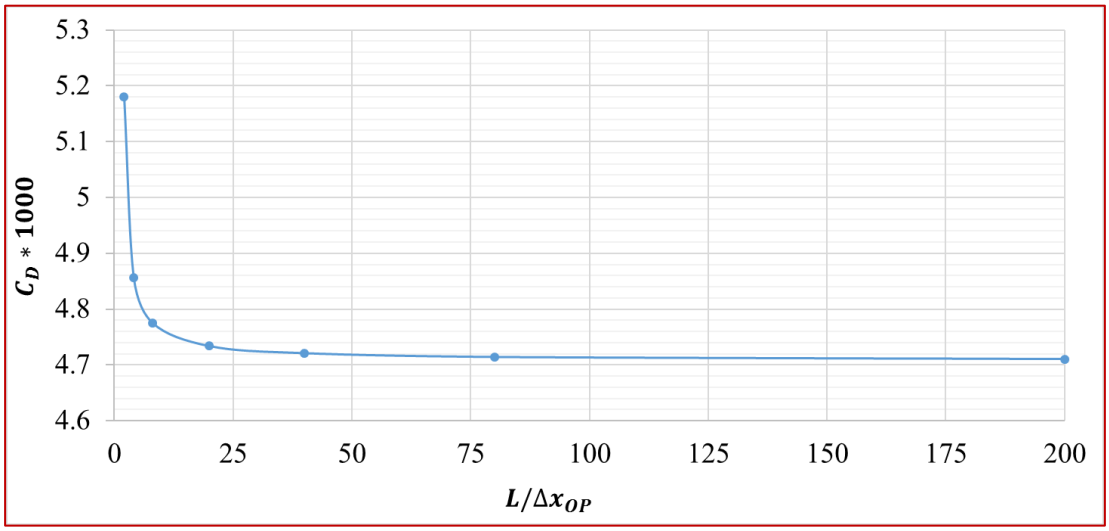

Figure 2.10 C_D values variation with respect to the different $L/\Delta x_{OP}$ values

Table 2.4 Mean skin-friction coefficient (C_D) values at the end of the plate for the different $L/\Delta x_{OP}$ values

Δx [mm]	$L/\Delta x_{OP}$	C_D values for 2 m	Calculation time [s]
1000	2	0.005180008	3.8
500	4	0.004856939	12.9
250	8	0.004774955	31.7
100	20	0.00473371	90.5
50	40	0.00472102	186.0
25	80	0.00471432	377.7
10	200	0.00471054	992.4

Table 2.5 The computation time reductions and the errors for the different $L/\Delta x_{OP}$ values with respect to (wrt) its grid independent value (200)

Δx [mm]	$L/\Delta x_{OP}$	Calculation time [s]	Error wrt $L/\Delta x_{OP}$ value of 200 [%]	Calc. time reduction wrt $L/\Delta x_{OP}$ value of 200 [times]
1000	2	3.8	9.06	260.1
500	4	12.9	3.01	76.9
250	8	31.7	1.35	31.3
100	20	90.5	0.49	11.0
50	40	186.0	0.22	5.3
25	80	377.7	0.08	2.6
10	200	992.4	0.00	1.0

In the study of grid independence; for the SPs, the $L/\Delta x_{SP}$ value of 10 brings error less than 1% in C_f with respect to $L/\Delta x_{SP}$ grid independent value which is 4000. For the OPs, the $L/\Delta x_{OP}$ value of 10 brings error less than 1.35% in C_D with respect to $L/\Delta x_{OP}$ grid independent value which is 200. Therefore, in the developed code, for both the $L/\Delta x_{SP}$ and $L/\Delta x_{OP}$ values, the number of 10 is used.

CHAPTER 3

COMPARISON OF THE PRESENT STUDY

Comparison of the present study is performed with the experimental works [13], [14], [31]–[34] and another numerical study in the literature that is Cebeci and Chang's work [16] in which the calculation of TBL parameters for incompressible fluids is performed.

3.1 Evaluation of the Comparison Data

For comparison study, it is essential to find experimental works which provide initial conditions (δ_2, C_f, ϖ), fluid and flow properties ($\overline{U}_E$, ν) and k_s value of the rough surface. In the literature survey, two studies are encountered which possess substantial information.

One of them is the study of Cebeci and Chang [16] which is a numerical calculation of rough TBL for incompressible fluids. To compare their numerical study, Cebeci and Chang chose seven different experimental works. According to Cebeci and Chang, these experimental studies are particularly chosen because the works supply a wide range of free-stream conditions and geometries. Furthermore, they give enough information to generate initial data at the starting point which helps to avoid the uncertainties error related to predicted initial values.

Out of seven experimental studies, only five are evaluated as suitable for the comparison purpose. Because, remaining studies are about the TF with a pressure

gradient. Furthermore, these four experimental works supply eleven different flow cases for the comparison purpose of the present study.

The other study encountered in the literature survey belongs to Pimenta et al.'s [34]. In their work, there are three main objectives. The most important one for the present study is to provide documentation of the heat-transfer and the hydrodynamic measurement data to generate new and more advanced TBL prediction model. In their experimental works, three different flow cases are evaluated as suitable for the comparison purpose of the present study.

In total, fourteen different flow cases are assessed as appropriate comparison aim. All are about TF of incompressible fluids over a rough flat plate with zero pressure gradient. However, most of them do not specifically target to calculate TBL parameters. For instance, in the study of Arndt and Ippen [14], it is aimed to understand the cavitation phenomenon associated with bubble dynamics in TBL and its effect on the skin-friction coefficient. Yet, these kinds of studies also provide information about TBL parameters. Such experimental work belongs to Arndt and Ippen [14], Scottron and Power [33], Bettermann [13], Liu et al. [32], Coleman [31] and Pimenta et al. [34].

Except for the work of Pimenta et al., remaining studies partially provide relevant initial information for the present study. Therefore; k_s, δ_2 and ϖ have to be calculated by the researchers. Values of k_s, δ_2 are presented in the Cebeci and Chang's numerical study [16], and calculation methods are explained briefly in the paper as well. Yet, ϖ values which are needed as an input for the present study, are still unanswered.

Approaching to obtain initial values of the ϖ by making assumptions, information deficiency related to the ϖ is overcome. Nevertheless, it should be noted that such lack of information situation for k_s, δ_2, ϖ and trying to complete them by assumptions and calculations brings some amount of errors. However, because one of the fundamental objectives of Pimenta et al.'s study is to provide data to generate new and more advanced TBL prediction models, all the parameters, properties and the features interested in the presented code are clearly found in Pimenta et al.'s work. Therefore,

large incompatibility is not expected to be encountered while comparing the present study with Pimenta et al.'s work.

3.2 Evaluation of the Results

The local and mean C_f value is one of the main physical quantities relevant to engineering purposes, and $\delta, \delta_1, \delta_2$ are the integral-lengths which help to compute C_f. Hence, most part of the results section is covered with the comparison of C_f values, and results are submitted as graphs. Other computed TBL parameters results, such as $\delta, \delta_1, \delta_2$ are presented as a table, in Table 3.1. However, because there is no comparison of δ except for the Pimenta et al.'s study, only its value at the end of the plate is presented.

There are four curves on each graph with which the comparison results of the C_f values are expressed. The orange, blue, grey and yellow color ones stand for the C_f results of the present study, experimental measurements, Cebeci and Chang's numerical work and Schlichting skin-friction formula, Eqn. (1.5) respectively.

Error calculation of the present work, Cebeci and Chang's study [16] and Schlichting skin-friction formulation (1.5) with respect to experimental data are performed based on relative mean discretization error (RMDE), which is given as:

$$RMDE = \frac{1}{n} \sum_{i=1}^{n} \frac{\left| C_{f\_\text{comp}} - C_{f\_\text{exp}} \right|}{C_{f\_\text{exp}}} \tag{3.1}$$

where;

n : total number of OPs,

C_{f_comp} : C_f values that are compared with the experiment results,

C_{f_exp} : C_f values obtained from the experimental results.

RMDEs for the specific locations (OPs) on the flat plate (which are expressed as a marker on the curves in the each C_f results graphs) are calculated. These points are specifically chosen, because the TBL parameters data in the experimental studies are measured on them.

3.2.1 Results of Skin-Friction Coefficient

(i) Experimental Data from Arndt and Ippen's Study

In Arndt and Ippen's study [14], the free-stream velocity is kept constant and the surface roughness is varied as presented in the figures below. All experiment cases are conducted for fully-rough flow regime where the $k_s^+ > 70$.

For the first case, presented in Figure 3.1; RMDE for the local skin-friction value, C_f, is about 1.5% between the experimental data and the present study whereas it is 1.9% for the experiment and Cebeci and Chang's numerical study [16]. On the other hand, the maximum discrepancy values are 3.7% for the present study and 4.7% for the numerical study.

Furthermore, according to the result of the present study, the k_s^+ values change from 214 to 209 and the x/k_s values change from 1320 to 1878. Therefore, the experimental data and Schlichting skin-friction formulation, Eqn. (1.5) can be compared. Results show that the RMDE between the experiment and Schlichting formulation is about 41.1% for the C_f value.

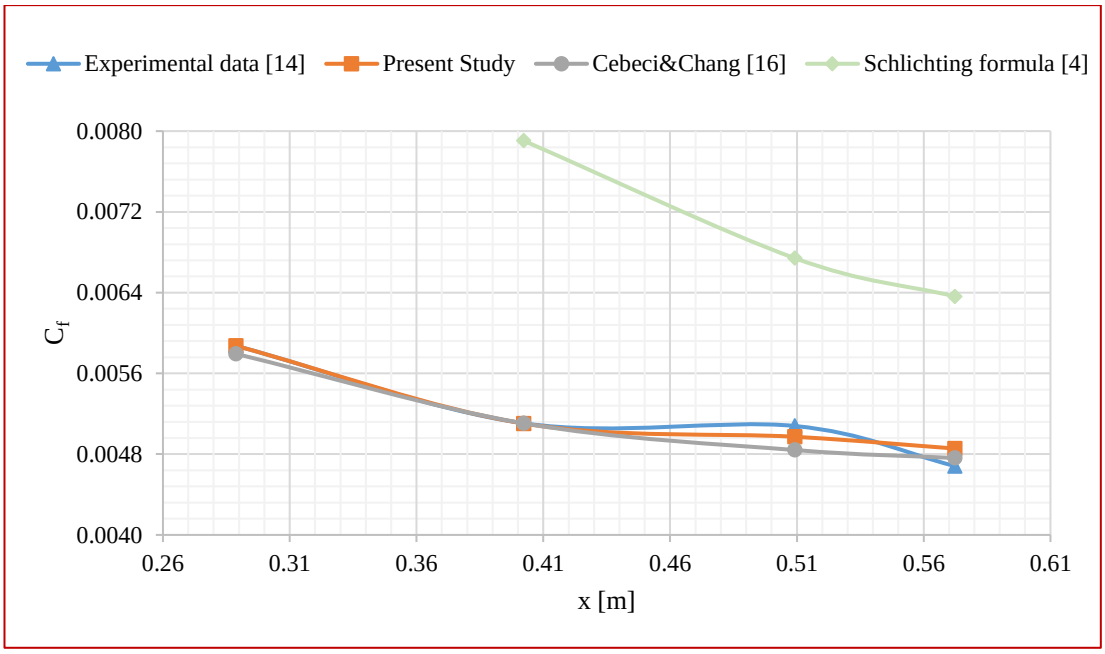

Figure 3.1 Results of Arndt and Ippen's experiment: U_E=12.27 m/s, k_s=0.3048 mm, ν=8.83x10^{-7} m^2/s, Re=8.47x10^6

For the second case, presented in Figure 3.2; the RMDE for the C_f is about 7.4% between the experimental data and the present study whereas it is 3.1% for the experimental data and Cebeci and Chang's numerical study [16]. On the other hand, the maximum discrepancy values are 15.8% for the present study and 8% for the numerical study.

Furthermore, according to the result of the present study, the k_s^+ values change from 574 to 552 and the x/k_s values change from 578 to 820. The RMDE for the C_f is about 41.0% between the experimental data and Schlichting formulation, Eqn. (1.5).

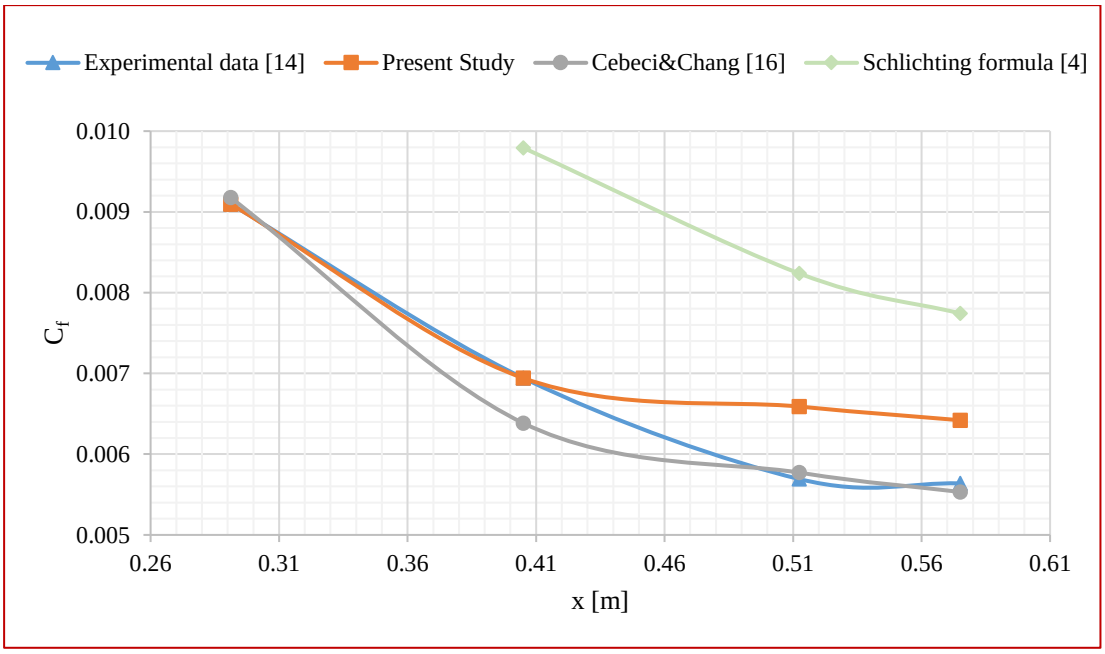

Figure 3.2 Results of Arndt and Ippen's experiment: U_E=12.27 m/s, k_s=0.7010 mm, ν=8.83x10^{-7} m^2/s, Re=8.47x10^6

For the third and the last case, presented in Figure 3.3; the RMDE for the C_f is about 2.0% between the experimental data and the present study whereas it is 2.1% for the experimental data and Cebeci and Chang's numerical study [16]. On the other hand, the maximum discrepancy values are 4.0% for the present study and 5.5% for the numerical study.

Furthermore, according to the result of the present study, the k_s^+ values change from 2354 to 2248 and the x/k_s values change from 161 to 229. The RMDE for the C_f is about 25.8% between the experimental data and Schlichting's formulation, Eqn.(1.5).

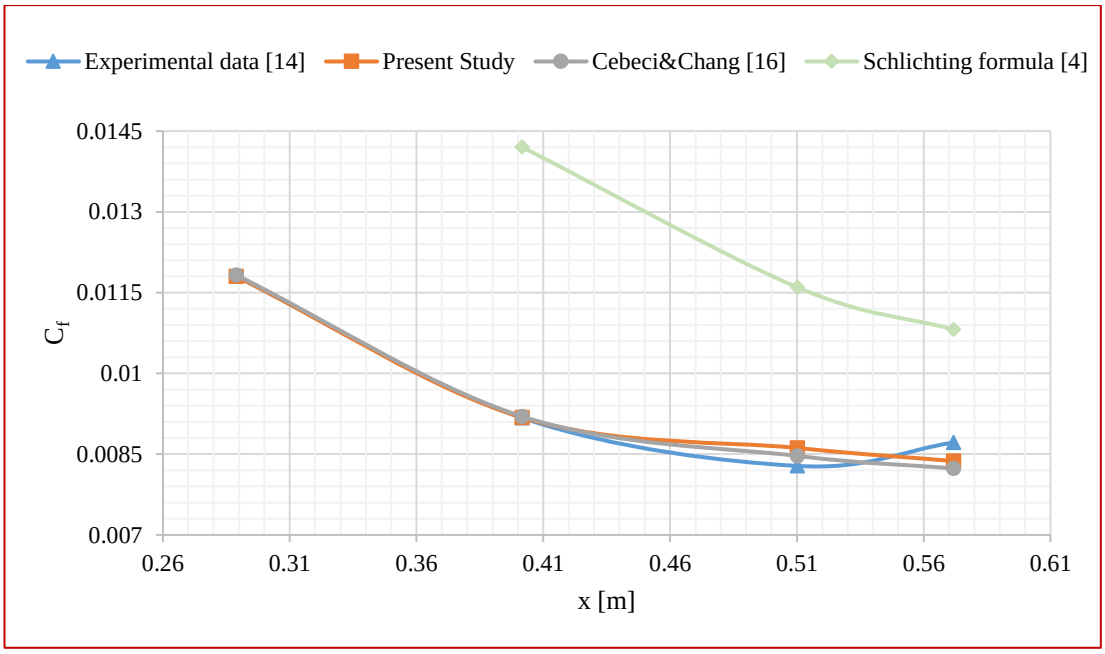

Figure 3.3 Results of Arndt and Ippen's experiment: U_E=12.27 m/s, k_s=2.5 mm, ν=8.83x10^{-7} m^2/s, Re=8.47x10^6

(ii) Experimental Data from Bettermann's Study

In Bettermann study [13], the free-stream velocity is kept constant and the surface roughness is varied just like the cases examined in the work of Arndt and Ippen. The experiments are conducted for fully-rough flow regime where the $k_s^+ > 70$ in their study.

For the first case, presented in Figure 3.4; the RMDE for the C_f is about 5.3% between the experimental data and the present study whereas it is 1.6% for the experimental data and Cebeci and Chang's numerical study [16]. On the other hand, the maximum discrepancy values are 9.6% for the present study and 3.4% for the numerical study.

Furthermore, according to the result of the present study, the k_s^+ values change from 151 to 142 and the x/k_s values change from 394 to 909. The RMDE for the C_f is about 50.8% between the experimental data and Schlichting formulation, Eqn. (1.5).

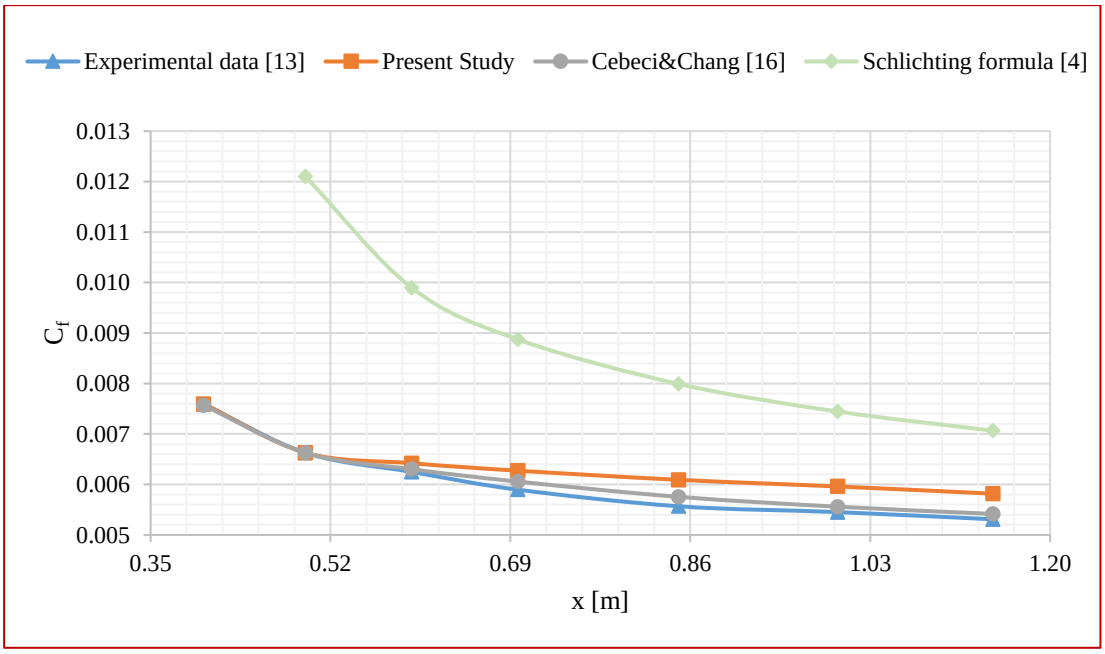

Figure 3.4 Results of Bettermann's experiment: U_E=30 m/s, k_s=1.26 mm, ν=1.44x10^{-5} m^2/s, Re=2.50x10^6

For the second case, presented in Figure 3.5; the RMDE for the C_f is about 2.5% between the experimental data and the present study which has the same value for Cebeci and Chang's numerical study [16] with respect to experimental study. On the other hand, the maximum discrepancy values are 4.6% for the present study and 3.6% for the numerical study.

Furthermore, according to the result of the present study, the k_s^+ values change from 513 to 480 and the x/k_s values change from 131 to 303. The RMDE for C_f is about 48.5% between the experimental data and Schlichting's formulation Eqn. (1.5).

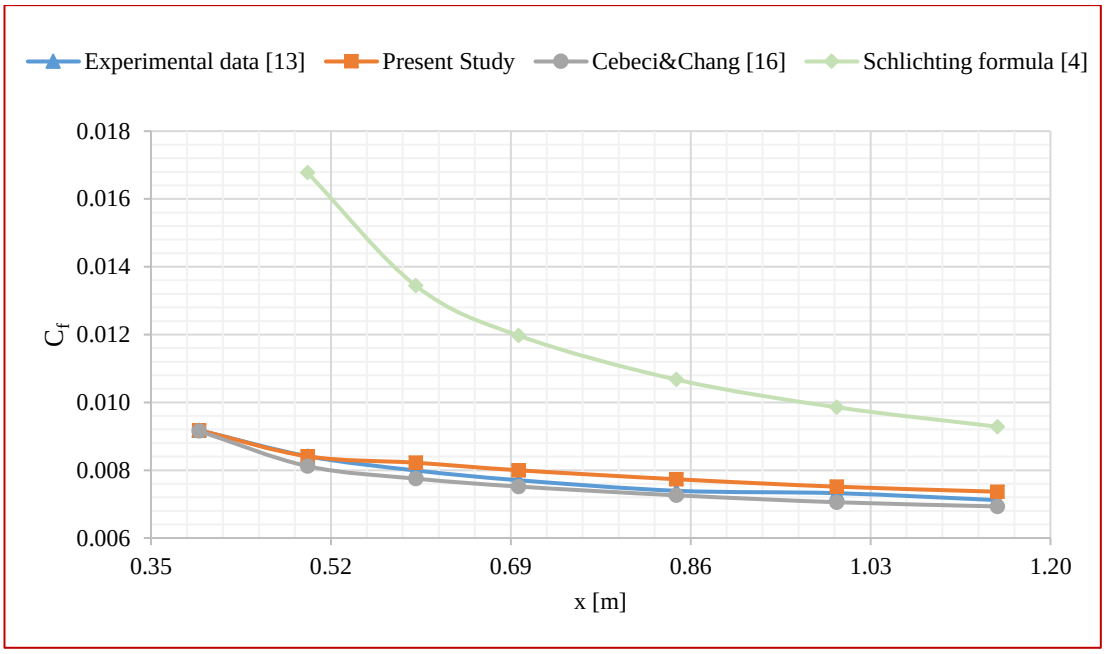

Figure 3.5 Results of Bettermann's experiment: U_E=30 m/s, k_s=3.80 mm, ν=1.44x10^{-5} m^2/s, Re=2.50x10^6

For the third and the last case examined, presented in Figure 3.6; the RMDE for the C_f is about 3.0% between the experimental data and the present study whereas it is 0.6% for the experimental data and Cebeci and Chang's numerical study [16]. On the other hand, the maximum discrepancy values are 6.7% for the present study and 1.6% for the numerical study.

Furthermore, according to the result of the present study, the k_s^+ values change from 1409 to 1308 and the x/k_s values change from 54 to 124. Although parts of the range of the x/k_s values are out of the validity limit of Schlichting skin-friction formulation, the RMDE is presented at least to give an idea. The RMDE for the C_f is about 65.2% between Schlichting formulation, Eqn. (1.5), and the experimental data.

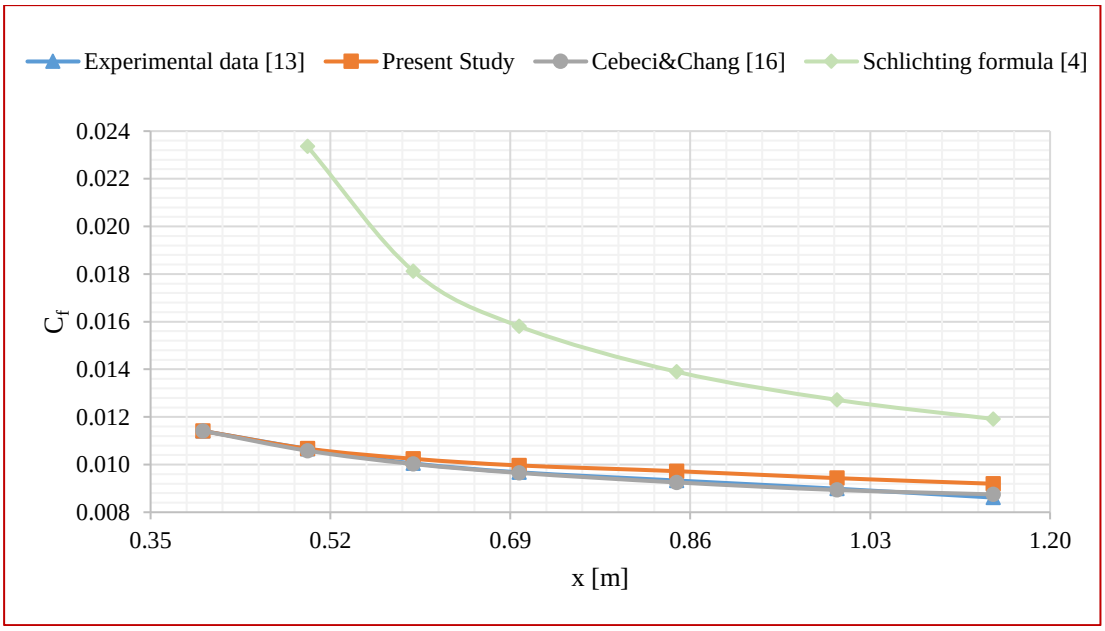

Figure 3.6 Results of Bettermann's experiment: U_E=30 m/s, k_s=9.26 mm, ν=1.44x10^{-5} m^2/s, Re=2.50x10^6

(iii) Experimental Data from Coleman's Study

In Coleman work [31], there is only one case which can be used for the comparison purpose of the present study. If one refers to his original paper, there is more than one case which includes the flow with pressure gradient as well. Furthermore, all the experiments he performed cover the fully-rough flow regime.

In the considered case, presented in Figure 3.7; the RMDE for the C_f is about 2.4% between the experimental data and the present study whereas it is 2.7% for the experimental data and Cebeci and Chang's numerical study [16]. On the other hand, the maximum discrepancy values are 5.7% for the present study and 3.0% for the numerical study.

Furthermore, according to the result of the present study, the k_s^+ values change from 75 to 70 and the x/k_s values change from 593 to 1493. The RMDE for the C_f is about 36.5% between the experimental data and Schlichting's formulation, Eqn. (1.5).

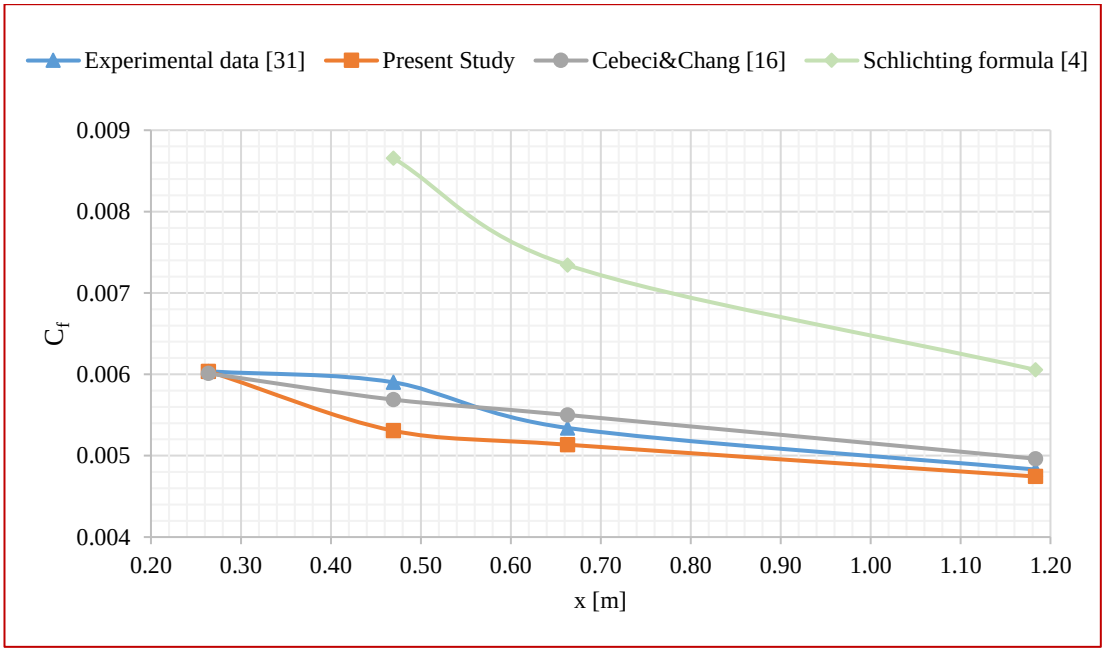

Figure 3.7 Results of Coleman's experiment: U_E=26.43 m/s, k_s=0.7925 mm, ν=1.51x10^{-5} m^2/s, Re=4.26x10^6

(iv) Experimental Data from Liu et al.'s Study

In Liu et al.'s work [32], the free-stream velocity is kept constant and the surface roughness value is changed. Such roughness difference is performed not by changing the roughness height but by changing the roughness density. Reynolds numbers of experiments are relatively low and resulting values of the k_s^+ change from 20 to over 100 in which some parts of the range include transition flow regime. Therefore, Liu et al's experimental data help to test the present study for low Re and also for the transition flow regime.

For the first case, presented in Figure 3.8; the RMDE for the C_f is about 4.7% between the experimental data and the present study whereas it is 5.4% for the experimental data and Cebeci and Chang's numerical study [16]. Because calculated k_s^+ value is approximately 25, and the k_s value is the lowest one in the experimental data, this case is thought to serve as a test case representing the transition flow regime. On the other hand, the maximum discrepancy values are 13.3% for the present study and 12.1% for the numerical study.

Furthermore, the x/k_s values change from 527 to 1126. Since the flow regime is not fully-rough, the validity of Schlichting's formulation is not expected. Nevertheless, the RMDE is submitted to give an idea. The RMDE for the C_f is about 44.1% between the experiment and Schlichting's formulation, Eqn. (1.5).

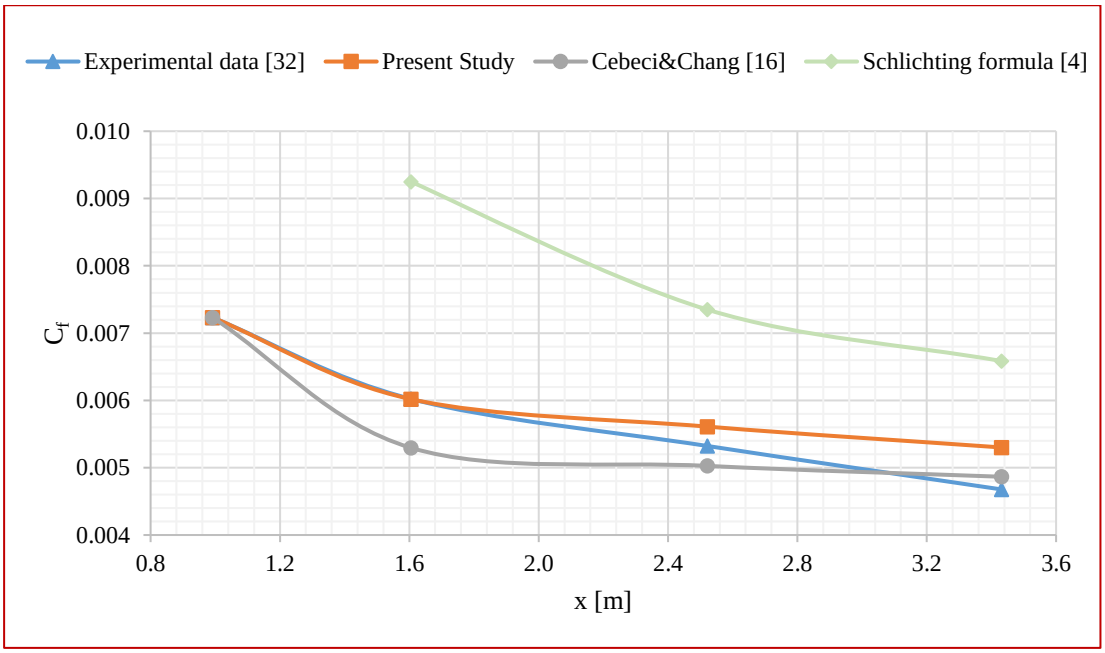

Figure 3.8 Results of Liu et al.'s experiment: U_E=0.15 m/s, k_s=3.05 mm, ν=9.66x10^{-7} m^2/s, Re=5.77x10^5

For the second case, presented in Figure 3.9; the RMDE, for the C_f is about 7.2% between the experimental data and the present study whereas it is 5.7% for the experimental data and Cebeci and Chang's numerical study [16]. On the other hand, the maximum discrepancy values are 16.7% for the present study and 10.3% for the numerical study.

Furthermore, according to the result of the present study, the k_s^+ values change from 147 to 137 and the x/k_s values change from 115 to 246. The RMDE for the C_f is about 41.0% between the experimental data and Schlichting's formulation, Eqn. (1.5).

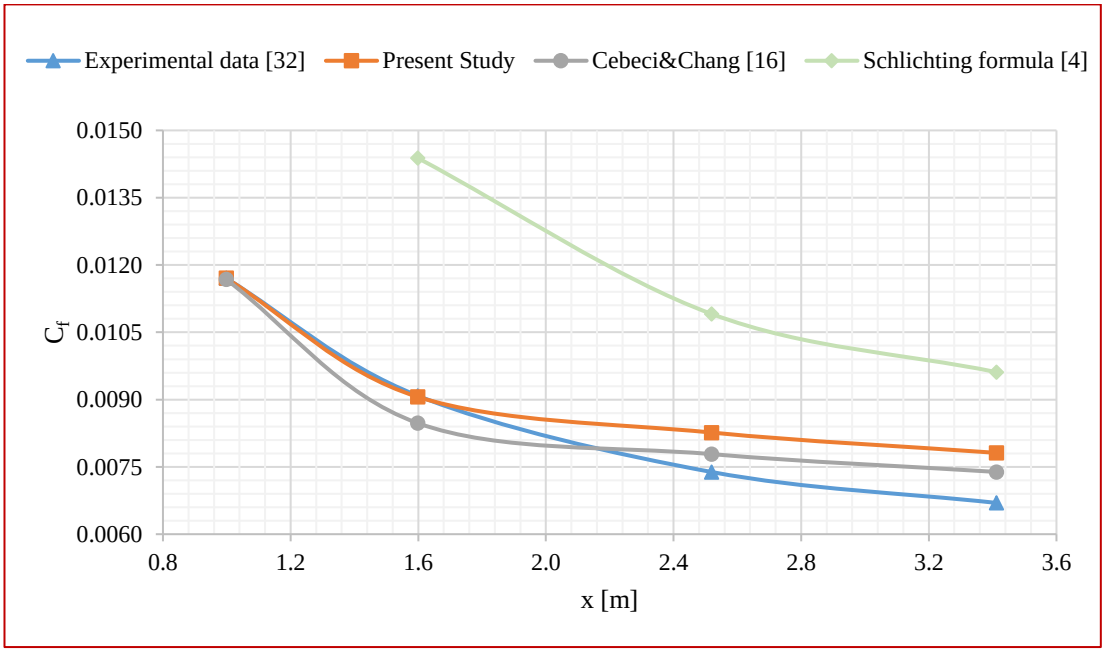

Figure 3.9 Results of Liu et al.'s experiment: U_E=0.15 m/s, k_s=13.87 mm, ν=9.66x10^{-7} m^2/s, Re=5.77x10^5

(v) Experimental Data from Scottron and Power's Study

In this experimental work of Scottron and Power [33]; whereas the surface roughness is kept constant, the free-stream velocity is changed. All relevant experiments are conducted for fully-rough flow regime where the $k_s^+ > 70$ in their study.

For the first case, presented in Figure 3.10; the RMDE for the C_f is about 0.8% between the experimental data and the present study whereas it is 2.8% for the experimental data and Cebeci and Chang's numerical study [16]. On the other hand, the maximum discrepancy values are 1.8% for the present study and 5.6% for the numerical study.

Furthermore, according to the result of the present study, the k_s^+ values change from 578 to 535 and the x/k_s values change from 176 to 354. The RMDE for the C_f is about 52.6% between the experimental data and Schlichting's formulation, Eqn. (1.5).

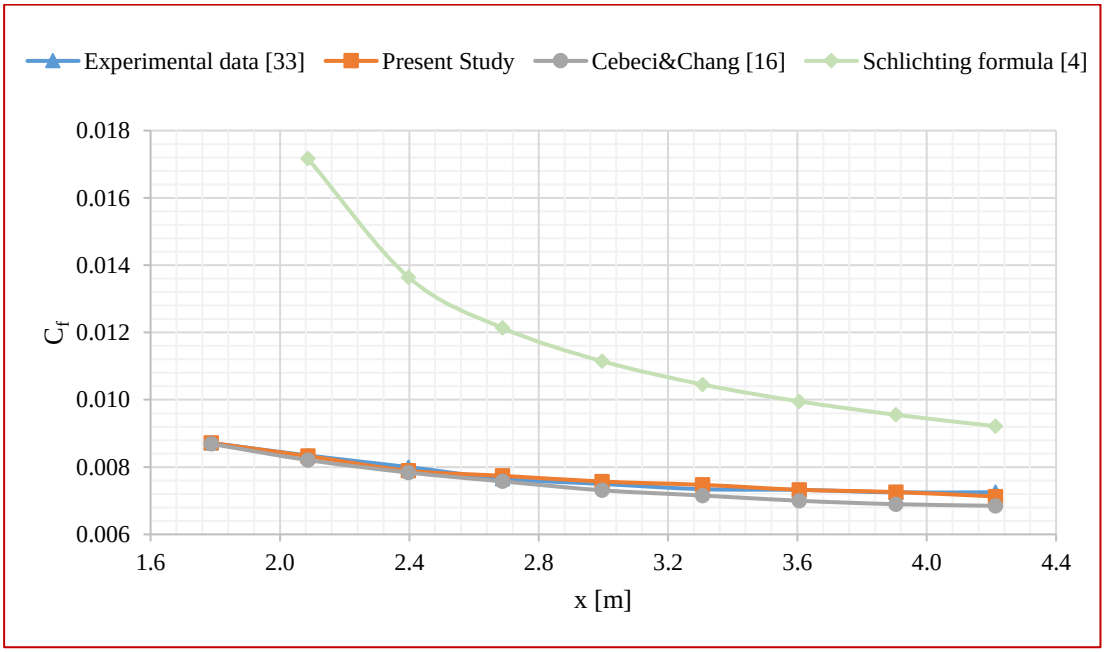

Figure 3.10 Results of Scottron and Power's experiment: U_E=11.28 m/s, k_s=11.89 mm, ν=1.50x10^{-5} m^2/s, Re=3.22x10^6

For the second case, presented in Figure 3.11; the RMDE for the C_f is about 1.5% between the experimental data and the present study whereas it is 3.8% for the experimental data and Cebeci and Chang's numerical study [16]. On the other hand, the maximum discrepancy values are 6.2% for the present study and 5.4% for the numerical study.

Furthermore, according to the result of the present study, the k_s^+ values change from 1047 to 968 and the x/k_s values change from 176 to 354. The RMDE for the C_f is about 57.0% between the experimental data and Schlichting's formulation, Eqn.(1.5).

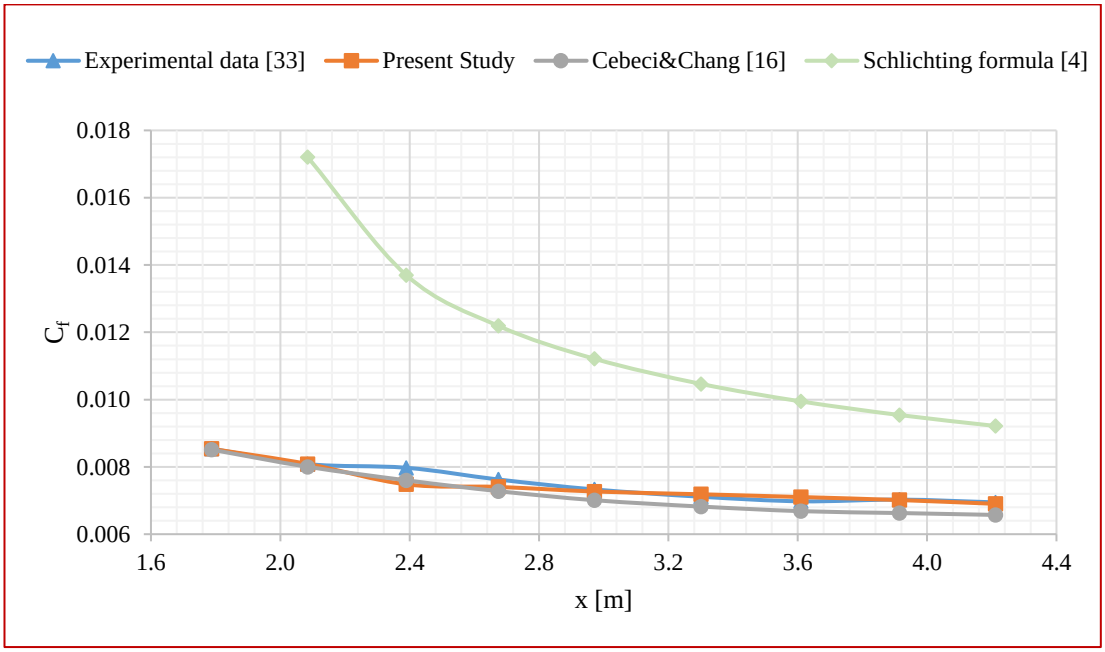

Figure 3.11 Results of Scottron and Power's experiment: U_E=20.73 m/s, k_s=11.89 mm, ν=1.50x10^{-5} m^2/s, Re=5.91x10^6

(vi) Experimental Data from Pimenta et al.'s Study

Pimenta et al. conduct an experimental study [34] in which rough surfaces are examined for isothermal and non-isothermal, zero pressure gradient flows with and without blowing (or transpiration). In addition to flow in the fully-rough flow regime, the transitionally flow rough regime is also investigated. They perform the experiments at three different velocities, 15.8 m/s, 27.1 m/s, 39.6 m/s. While the lowest one serves for the transitionally-rough flow regime, the other two are for fully-rough flow regimes. By maintaining the maximum flow velocity below 39.6 m/s, they ensure that they are able to use constant fluid properties, which can vary due to the high velocities.

For the first case, which serves for the transition flow regime, presented in Figure 3.12; the RMDE for the C_f is about 1.9% between the experimental data and the present study whereas it is 8% for the experimental data and Cebeci and Chang's numerical study [16]. On the other hand, the maximum discrepancy values are 4.1% for the present study and 11.4% for the numerical study.

Furthermore, according to the result of the present study, the k_s^+ values change from 42 to 39 and the x/k_s values change from 1149 to 2674. Although Schlichting's skin-friction formulation, Eqn. (1.5) is not valid for this regime, the RMDE is still submitted to give an idea for the transition state. The RMDE for the C_f is about 29.0% between the experimental data and Schlichting's formulation.

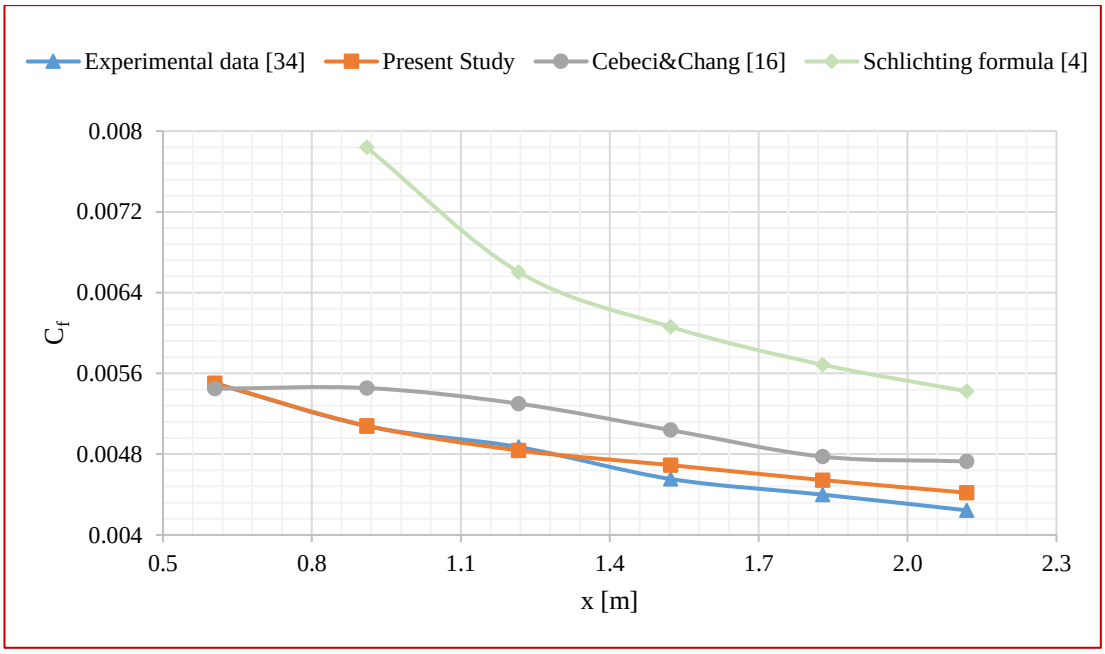

Figure 3.12 Results of Pimenta et al.'s experiment: U_E=15.84 m/s, k_s=0.7925 mm, ν=1.50x10^{-5} m^2/s, Re=2.58x10^6

For the second case, which serves for the fully-rough flow regime, presented in Figure 3.13; the RMDE for the C_f is about 1.0% between the experimental data and the present study whereas it is 3% for the experimental data and Cebeci and Chang's numerical study [16]. On the other hand, the maximum discrepancy values are 2.9% for the present study and 5.1% for the numerical study.

Furthermore, according to the result of the present study the, k_s^+ values change from 72 to 68 and the x/k_s values change from 1152 to 2692. The RMDE for the C_f is about 35.0% between the experimental data and Schlichting formulation, Eqn. (1.5).

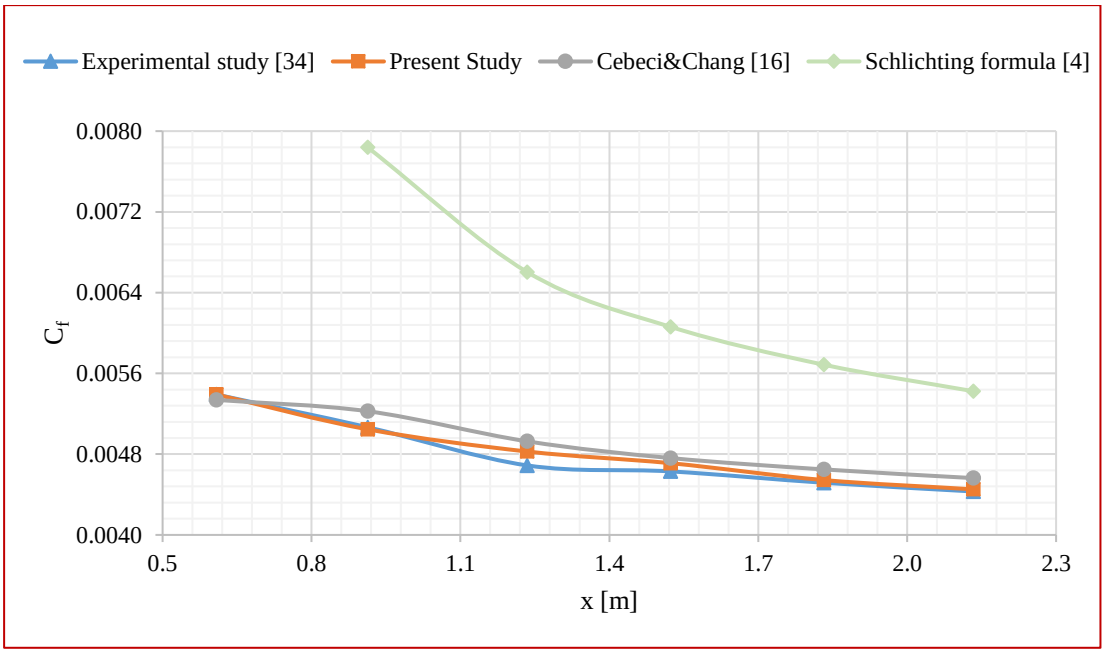

Figure 3.13 Results of Pimenta et al.'s experiment: U_E=27.13 m/s, k_s=0.7925 mm, ν=1.50x10^{-5} m^2/s, Re=4.42x10^6

For the third and the last case, which serves for the fully-rough flow regime, presented in Figure 3.14; the RMDE for the C_f is about 0.6% between the experimental data and the present study whereas it is 2.1% for the experimental data and Cebeci and Chang's numerical study [16]. On the other hand, the maximum discrepancy values are 1.8% for the present study and 4.4% for the numerical study.

Furthermore, according to the result of the present study, the k_s^+ values change from 105 to 99 and the x/k_s values change from 1139 to 2687. The RMDE for the C_f is about 33.8% between the experiment and Schlichting's formulation, Eqn. (1.5).

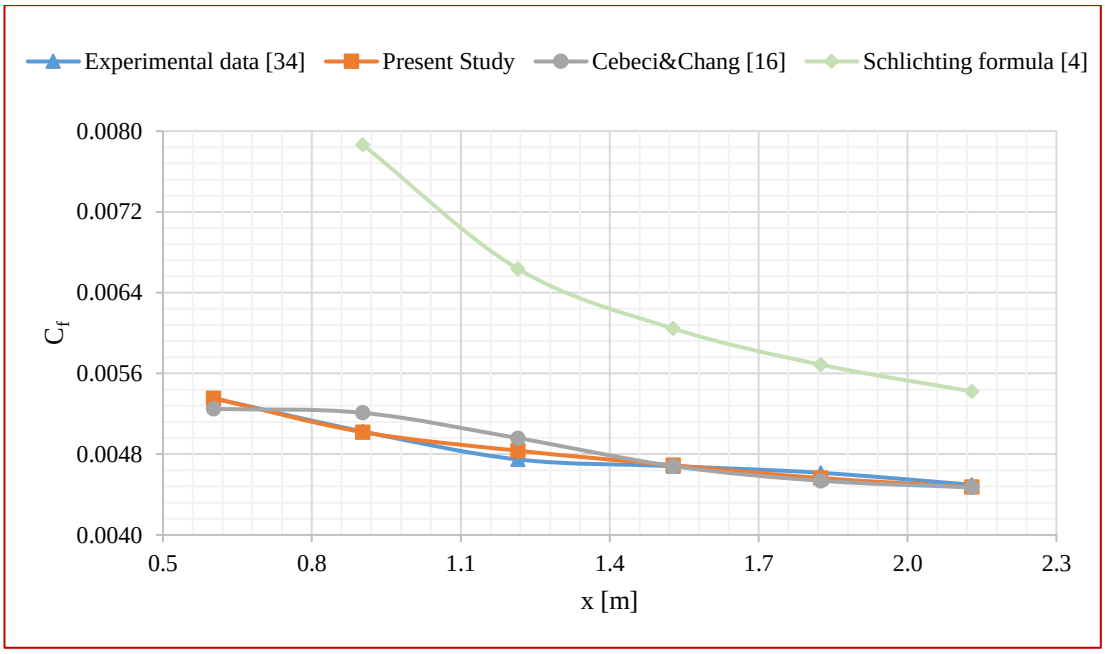

Figure 3.14 Results of Pimenta et al.'s experiment: U_E=39.62 m/s, k_s=0.7925 mm, ν=1.50x10^{-5} m^2/s, Re=6.46x10^6

3.2.2 Results of TBL, Displacement and Momentum Thicknesses

As mention at the beginning of Section 3.2; except for the skin-friction coefficient, TBL parameters results, such as δ , δ_1, δ_2 are presented as a table, in Table 3.1.

Table 3.1 δ , δ_1, δ_2 results and the methods to obtain the initial values

Experiments	Flow regime	δ values at the end of the plate[mm]	RMDE of the δ_1 [%]		RMDE of the δ_2 [%]		Initial values obtaining method			
		Present study	Present study & Experiment	Cebeci&Chang & Experiment	Present study & Experiment	Cebeci&Chang & Experiment	C_f	ϖ	δ_2	k_s
Arndt&Ippen Case-1	Fully-rough	14.9	2.0	3.3	0.8	2.4	Given	Assumed	Given	Calculated
Arndt&Ippen Case-2	Fully-rough	18.0	0.8	3.3	4.2	0.3	Given	Assumed	Given	Calculated
Arndt&Ippen Case-3	Fully-rough	20.4	6.1	2.5	7.6	0.8	Given	Assumed	Given	Calculated
Bettermann Case-1	Fully-rough	39.8	1.3	1.7	2.2	1.9	Given	Assumed	Given	Calculated
Bettermann Case-2	Fully-rough	44.3	3.8	0.5	0.7	0.6	Given	Assumed	Given	Calculated
Bettermann Case-3	Fully-rough	50.1	6.8	4.7	1.4	0.8	Given	Assumed	Given	Calculated
Coleman Case-1	Fully-rough	32.3	1.7	1.5	2.1	1.3	Given	Assumed	Given	Given
Liu et al. Case-1	Transition	111.7	2.4	2.9	4.1	2.2	Given	Assumed	Given	Calculated
Liu et al. Case-2	Fully-rough	132.2	3.5	0.8	3.5	1.6	Given	Assumed	Given	Calculated
Scottron&Power Case-1	Fully-rough	155.3	2.1	1.3	0.9	1.1	Given	Assumed	Given	Calculated
Scottron&Power Case-2	Fully-rough	152.3	4.0	1.6	1.7	1.3	Given	Assumed	Given	Calculated
Pimenta et al. Case-1	Transition	45.4	3.5	1.8	2.7	1.3	Given	Given	Given	Given
Pimenta et al. Case-2	Fully-rough	49.1	1.7	0.8	1.7	0.8	Given	Given	Given	Given
Pimenta et al. Case-3	Fully-rough	50.0	1.4	0.9	1.6	1.1	Given	Given	Given	Given

CHAPTER 4

DISCUSSION AND CONCLUSION

One of the most important characteristics of the present work to obtain the TBL parameter precisely, the solution technique considers the TBL developing. According to such consideration, the relative size of sublayers thicknesses in a TBL and surface roughness height with respect to each other is a crucial matter to obtain the correct values of TBL parameters.

Another characteristic of the present study is that fluid mechanics formulations, such as momentum integral equation are coupled with the results of Nikuradse's experiment. These formulations form a different system of equations compared to the works to solve TBL in the literature.

4.1 Discussion of the Results

Most of the results of the present study show that there is good agreement with the experimental results. The compatibility is at its highest level when full experimental data of references were available, such as being in Pimenta et al.'s study. Because, in those cases, it was not necessary to make any assumption. For other cases where the full experimental data was not available, it was necessary to make some assumptions as related to the equations used in the present study. Normally, for the latter cases, it is had to be assumed either the equivalent sand roughness or some parameters, or both.

Wake parameter, ϖ, has a high impact on the calculation of TBL parameters. Except for the Pimenta et al.'s experimental study, an approach is used to obtain its initial

value. According to the approach, the initial values of ϖ are obtained by changing its value until the measured (experimental) C_f and calculated C_f values match with each other. The same treatment can also be observed in T. Cebeci and C. Chang's work. Furthermore, again except for the study of Pimenta et al, equivalent sand roughness is not defined as k_s in the experimental works used for comparison. Hence, all roughness length scales presented in the experimental studies are converted to k_s by using Dvorak's correlation [12].

Such approaching and calculations about ϖ and k_s are obligated to be performed since the experiments main purpose is not to provide data for the numerical calculation of TBL. Hence, they are calculated by the researchers. As a result, these the approaching and calculations bring some amount of error. Another possible error factor may be the inaccuracy of processing experimental data from graphs in which they are submitted.

However, in the study of Pimenta et al., because one of the main objectives is to provide data which help to generate new and more advanced TBL prediction models, full experimental data is clearly found in Pimenta et al.'s work. Hence, incompatibility due to the lack of information is not expected to be encountered while comparing Pimenta et al.'s study and the present work. As a result; the best conformality with experimental cases and the comparison with Cebeci and Chang's numerical study is achieved by using Pimenta et al.'s measurement data.

For the fully-rough flow regime, the present study gives the RMDE in C_f as 0.6% according to the comparison result of it with Pimenta et al.'s experimental work whereas it is 2.1% according to the comparison result of Cebeci and Chang's numerical study with Pimenta et al.'s experimental work. For the transition flow regime, the the RMDE in C_f is found to be 1.9% in the present work and it is 8.0% for Cebeci and Chang's numerical study when they are compared with Pimenta et al.'s experimental study.

Schlichting's skin-friction formula, Eqn. (1.5) overestimates the skin-friction value, and accordingly the frictional drag occurring in reality. An explanation of this situation can be done by considering the F. Schultz-Grunow [29] experimental study.

According to the F. Schultz-Grunow's experimental results that the velocity profile in the outer portion of the boundary layer of a plate deviates from the logarithmic velocity distribution inside a circular pipe with respect to his measurement on the boundary layer for a plate as presented in Figure 1.3 [4]. By considering the velocity-defect formulation as momentum loss in TBL (that is frictional drag), the C_f values (which are obtained for the flat plate directly from the J. Nikuradse pipe flow experiments by the analogy) should be higher than that of the experimental results for a flat plate.

The physical reason behind such phenomenon may be that the methodology for obtaining Schlichting's skin-friction formula, Eqn. (1.5), depends on the analogy between the pipe flow and the boundary layer flow by making the assumption that the velocity profile inside the pipe flow is similar to that of on the flat plate. While working with moderate Re, power-law can be used for both pipe and boundary layer flow and the assumption keeps its validity. Hence, calculated C_f values are in accordance with experimental results. However, for arbitrarily large Re, using power-law is not appropriate and logarithmic-law should be used [4]. In the logarithmic-law, there is an additional term named wake function, W. It is responsible for the main difference between the pipe and the boundary layer flow velocity distribution. Because, the effect of the W increases while Re is rising, its impression becomes dominant on the velocity distribution at high Re. Hence, the applicability of the assumption, which is the velocity distribution in a pipe identical with that in the boundary layer on a plate, loses validity.

The RMDE in the local skin-friction coefficient, C_f, changes between 25.8% and 57% according to the comparison of experimental data and Schlichting's skin-friction formula. It should be noted that, because the constraints of Schlichting's skin-friction

formula, Liu et al. Case-1 and Pimenta et al. Case-1, and Bettermann's case-3 are not evaluated for comparison.

The ϖ changes throughout the flow. Such phenomenon brings the requirement of calculation of the ϖ for every SP just as the C_f is being calculated throughout the computation domain. Instead of computing the ϖ at every SP, it is calculated only some specific SPs named OPs. Therefore, time consumption for the numerical calculation is decreased. For this purpose, a method is developed during the present study, and it uses the relationship between the C_f and ϖ values. The calculation methodology of ϖ exhibits its success according to the comparison results.

In the study of grid independence; for the SPs, the $L/\Delta x_{SP}$ value of 10 brings error less than 1% in C_f with respect to $L/\Delta x_{SP}$ grid independent value which is 4000. For the OPs, the $L/\Delta x_{OP}$ value of 10 brings error less than 1.35% in C_D with respect to $L/\Delta x_{OP}$ grid independent value which is 200. The values of error both for C_f and C_D are quite acceptable.

In order to work with the developed code; firstly, Reynolds number based on plate length should be of the order of 10^6 or higher. Because, according to A. D. Young et al. [2] the form of velocity-defect law is acceptable for such Reynolds numbers.

Secondly, the mathematical model requires the knowledge of equivalent sand roughness, k_s . Hence, it is important to know the k_s value for the surface of interest.

Finally, as a remember, to find the value of the A', results of Nikuradse's experiment are used. In the experiments the k_s^+ value approximately change between 1.58 and 1584. This range covers most of the problems of the type consşdered in this work. Therefore the code has a big range applicability.

4.2 Concluding Remarks

The present study gave much better results when full experimental data of references were available.

As a future work, items below can be considered:

- Developed code can be improved for an attached TF over a rough surface with a pressure gradient.

- The developed code can be embedded into a CFD solver algorithm after having performed proper modifications on it if they are necessary.

- It may be possible to obtain a diagram that represents a qualitatively and quantitatively C_f better than Schlichting's diagram offers, which is still used in present-day engineering hand-calculations. Moreover, semiempirical local and mean C_f correlations for fully-rough flow regime can be developed by using the data of this diagram.

- TBL solution can be obtained for a complete plate which starts from laminar flow. However, transition regime of TF on a rough surface is expected to be short. If the conditions are such that transition of rough surface has a sizeable length; this problem is worth to be investigated on its own respect.

REFERENCES

[1] C. Çıray, *Akışkanlar Mekaniğine Giriş-1*, 1st ed. ODTÜ Yayıncılık, 2007.

[2] W. J. Duncan, A. S. Thom, and A. D. Young, *Mechanics of Fluids*, 2nd ed. 1970.

[3] C. Çıray, *Akışkanlar Mekaniğine Giriş-2*, 1st ed. ODTÜ Yayıncılık, 2010.

[4] H. Schlichting, *Boundary Layer Theory*, 4th ed. McGraw-Hill, 1960.

[5] T. Cebeci, J. P. Shao, F. Kafyeke, and E. Laurendeau, *Computational Fluid Dynamics for Engineers*. 2005.

[6] T. Cebeci and A. M. O. Smith, "Analysis of turbulent boundary layers," no. 1970, p. 404, 1974.

[7] C. Çıray, *Akışkanlar Mekaniğine Giriş-3*, 1st ed. ODTÜ Yayıncılık, 2013.

[8] T. V. Kármán, "Über laminare und turbulente Reibung," *ZAMM - J. Appl. Math. Mech. / Zeitschrift für Angew. Math. und Mech.*, vol. 1, no. 4, pp. 233–252, 1921.

[9] J. M. Burgers, "The Motion of a Fluid in the Boundary Layer along a Plane Smooth Surface," in *Congress for Applied Mechanics 121*, 1923.

[10] L. Prandtl and H. Schlichting, "The Resistance Law for Rough Plates," *Werft-Reederei-Hafen*, vol. 15, 1955.

[11] D. Bettermann, "Contribution a l'etude de la convection forcee turbulente le long de plaques rugueuses," *Int. J. Heat Mass Transf.*, vol. 9, no. 3, pp. 153–164, 1966.

[12] F. A. Dvorak, "Calculation of Turbulent Boundary Layers on Rough Surfaces in Pressure Gradient.," *AIAA J.*, 1969.

[13] D. Bettermann, "Contribution à l'étude de la couche limite turbulente le long de plaques rugueuses," vol. 65–6, 1965.

[14] R. E. A. Arndt and A. T. Ippen, "Rough Surface Effects on Cavitation Inception," *J. Basic Eng.*, vol. 90, no. 2, p. 249, 1968.

[15] T. Cebeci and P. Bradshaw, *Momentum Transfer in Boundary Layers*. Hemisphere Publishing Corporation, 1977.

[16] T. Cebeci and K. C. Chang, "Calculation of Incompressible Rough-Wall Boundary-Layer Flows," *AIAA J.*, 1978.

[17] P. Bradshaw, D. H. Ferriss, and N. P. Atwell, "Calculation of Boundary-Layer Development Using the Turbulent Energy Equation," *J. Fluid Mech.*, 1967.

[18] M. R. Head, "Entrainment in the Turbulent Boundary Layer," *Aero. Res. Counc. London*, vol. 3152, 1958.

[19] P. Bradshaw and D. H. Ferriss, "National Physical Laboratory Aerodynamics Report," 1965.

[20] R. A. Antonia and D. H. Wood, "Calculation of a Turbulent Boundary Layer Downstream of a Step Change in Surface Temperature," no. July, pp. 202–210, 1975.

[21] R. A. Antonia and R. E. Luxton, "Characteristics of Turbulence Within an Internal Boundary Layer," 1959.

[22] K. A. Flack and M. P. Schultz, "Roughness Effects on Wall-Bounded Turbulent Flows," *Phys. Fluids*, 2014.

[23] F. R. Hama, "Boundary-Layer Characteristics for Smooth and Rough Surfaces," *Trans. Soc. Nav. Arch. Mar. Engrs.*, vol. 62, pp. 333–358, 1954.

[24] F. H. Clauser, "Turbulent Boundary Layers in Adverse Pressure Gradients," *J. Aeronaut. Sci.*, vol. 21, pp. 91–108, 1954.

[25] A. Betz and J. C. Rotta, *Über die Theorie der turbulenten Grenzschichten*. Max-Planck-Inst. f. Strömungsforschg, 1950.

[26] T. Cebeci and P. Bradshaw, *Physical and Computational Aspects of Convective Heat Transfer*. Springer-Verlag, 1984.

[27] M. R. Doshi and W. N. Gill, "A Note on the Mixing Length Theory of Turbulent Flow," *AIChE J.*, vol. 16, no. 5, pp. 885–888, 1970.

[28] M. S. Yalın and A. M. A. F. Da Silva, *Fluvial Processes*. Delft, Netherlands, 2001.

[29] F. Schultz-Grunow, "New Frictional Resistance Law for Smooth Plates," 1940.

[30] D. Coles, "Measurements in the Boundary Layer on a Smooth Flat Plate in Supersonic Flow," 1953.

[31] H. W. Coleman, “Momentum and Energy Transport in the Accelerated Fully Rough Turbulent Boundary Layer,” Stanford Univ., 1976.

[32] C. K. Liu, S. J. Kline, and J. P. Johnston, “An Experimental Study of Turbulent Boundary Layers on Rough Walls,” 1966.

[33] V. E. Scottron and J. L. Power, “The Influence of Pressure Gradient on Turbulent Boundary Layer over Rough Surface,” 1965.

[34] M. M. Pimenta, R. J. Moffat, and W. M. Kays, “The Turbulent Boundary Layer: An Experimental Study of the Transport of Momentum and Heat with the Effect of Roughness,” no. May, 1975.

APPENDIX A

THE DEVELOPED CODE

The developed code is written by using “Python” programming language, and the “Jupyter Notebook” version 5.4.0 is used for the interactive computing environment. It is presented below in the text format.

```
# SI UNITS ARE USED



# Libraries used in the developed code

import numpy as np
import matplotlib.pyplot as plt
from scipy.optimize import curve_fit
import scipy.integrate as integrate
import time as tm



# Steps calculating the TBL parameters

def BLT(D2):
    D = D_lit_s * 3
    while True:
        leftF = D2 / D
        rightF = (c1 * (1 / (Ap + B * np.log(D / ks) + (2 * B * w)))) - (c2
* (1 / (Ap + B * np.log(D / ks) + (2 * B * w))) ** 2)
        D = D - 0.0001
        if (rightF - leftF <= 0):
            break
    return D
```

```
start = tm.time()

L_plate = 3
ml_Cf_y = []
ml_L = np.linspace(L_plate/10, L_plate, L_plate*10)

for element in ml_L:
    L = element

    first_iteration = True

    for j in [0, 1, 2]:

        if first_iteration == True:
            ml_w = [0.75]
            w = ml_w[-1]

        else:
            w = (Cf / ml_Cf[0]) * ml_w[-1]
            ml_w.append(w)

        Ue = 27.1272
        ks = 0.00079248
        k_vis = 0.00001495738944
        rho = 1.1770
        B = 2.5

        DX = 0.1

        result_c1 = integrate.quad(lambda x: (-2.5 * np.log(x) +  2 * 2.5 *
w * (1 - (np.sin(np.pi / 2 * x)) ** 2)) ** 1, 0,1)
        c1 = result_c1[0]
        result_c2 = integrate.quad(lambda x: (-2.5 * np.log(x) +  2 * 2.5 *
w * (1 - (np.sin(np.pi / 2 * x)) ** 2)) ** 2, 0,1)
        c2 = result_c2[0]

        ml_U_tau = []
```

```
        ml_Cf = [0.00539076]
        ml_Ap = []
        ml_ks_p = []
        ml_D = []
        ml_D1 = []
        ml_D2= [0.002052760944]

        Re = Ue * L / k_vis
        D_lit_s = (0.38 * L) / (Re ** ( 1 / 5))

        for element in np.arange(1, (L/DX + 1)):

            D2 = ml_D2[-1] + DX * (ml_Cf[-1] / 2)
            ml_D2.append(D2)

            Cf = ml_Cf[-1]

            U_tau = Ue * ((Cf / 2) ** 0.5)
            ks_p = ks * U_tau / k_vis
            Ap = (2.5 * np.log(ks_p) + 5.5) * np.exp(-0.0705 * (np.log(ks_p)
) ** 2.55) + 8.5 * (1 - np.exp(-0.0594 * ((np.log(ks_p)) ** 2.55)))
            D = BLT(D2)
            D1 = (D * c1 * (1 / (Ap + B * np.log(D / ks) + (2 * B * w))))

            Cf_c = 2 / (Ap + B * np.log(D / ks) + (2 * B * w)) ** 2

            if (abs((Cf_c - Cf) / Cf)) * 100 < 1:

                ml_Cf.append(Cf)
                ml_U_tau.append(U_tau)
                ml_ks_p.append(ks_p)
                ml_Ap.append(Ap)
                ml_D.append(D)
                ml_D1.append(D1)


            else:
                while True:
                    if (abs((Cf_c - Cf) / Cf)) * 100 < 1:
```

```
                        ml_Cf.append(Cf)
                        ml_U_tau.append(U_tau)
                        ml_ks_p.append(ks_p)
                        ml_Ap.append(Ap)
                        ml_D.append(D)
                        ml_D1.append(D1)

                        break

                    else:

                        Cf = Cf_c

                        U_tau = Ue * ((Cf / 2) ** 0.5)
                        ks_p = ks * U_tau / k_vis
                        Ap = (2.5 * np.log(ks_p) + 5.5) * np.exp(-0.0705 * (
np.log(ks_p)) ** 2.55) + 8.5 * (1 - np.exp(-0.0594 * ((np.log(ks_p)) ** 2.55
)))
                        D = BLT(D2)
                        D1 = (D * c1 * (1 / ((Ap + (B * np.log(D / ks)) + (2
* B * w)))))

                        Cf_c = 2 / (Ap + (B * np.log(D / ks)) + (2 * B * w)
) ** 2

                        continue

        first_iteration = False

        ml_Cf.pop(0)

    ml_Cf_y.append(Cf)




# Calculating the mean skin-friction value by integrating the computed local
skin-friction coefficient values with respect to the plate length
x = ml_L
y = ml_Cf_y
```

```
def fit_func(x, a, b, c, d, e):
    return a*x**4 + b*x**3 + c*x**2 + d*x + e

params = curve_fit(fit_func, x, y)
[a, b, c, d, e] = params[0]

result= integrate.quad(lambda x: a*x**4 + b*x**3 + c*x**2 + d*x + e, 0,L)
answer= result[0]

Cd = answer/L

print(Cd, D, D1, D2)
print(tm.time()-start)
```